Journal of Water Process Engineering 49 (2022) 103034

Contents lists available at ScienceDirect

Journal of Water Process Engineering

journal homepage: www.elsevier.com/locate/jwpe

Recent advances on the treatment of oil fields produced water by adsorption and advanced oxidation processes

T.S. Alomar [a], B.H. Hameed [a,*], M. Usman [b], F.A. Almomani [a], M.M. Ba-Abbad [c], M. Khraisheh [a]

[a] Department of Chemical Engineering, College of Engineering, Qatar University, P.O Box: 2713, Doha, Qatar
[b] PEIE Research Chair for the Development of Industrial Estates and Free Zones, Center for Environmental Studies and Research, Sultan Qaboos University, Al-Khoud 123, Oman
[c] Gas Processing Center, College of Engineering, Qatar University, P.O Box: 2713, Doha, Qatar

ARTICLE INFO

Keywords:
Produced water
Advanced oxidation processes
Adsorption
Integrated process
Organic content
Batch process

ABSTRACT

The handling and treatment of produced water (PW) generated during oil and gas extraction has continued to be a serious dilemma due to its large quantities and complex composition with variety of pollutants. In this review article, the treatment of PW using adsorption and advanced oxidation processes (AOP) and their integrated processes is analyzed and discussed, where the PW sources studied were both real and artificially contaminated PW. The role of different reaction parameters and their effect on the performance of these processes is critically evaluated. Furthermore, the existing research gaps were identified where it was found that there are insufficient studies on the integration of adsorption and advanced oxidation processes, but with the available literature, it was shown that integrated adsorption-advanced oxidation processes could be effectively used to treat produced water. It was deduced that further studies should target continuous columns (packed bed) rather than batch systems. Moreover, cost analysis and comparison should be carried out to see the feasibility of these systems. Also, innovative integrated technologies and efficient methods for the regeneration and reuse of these systems should be studied for their upscaling to industrial-scale applications.

1. Introduction

Produced water (PW) is wastewater produced as a by-product of upstream petroleum exploration and operation. It comprises a complex mixture with a rich amount of organic (hydrocarbons) and inorganic (heavy metals, sulphides) pollutants [1]. These pollutants are derived from chemical additives (surfactants), environmental pollutants (hardness and dissolved solids, radioactive material, microorganism) and residual oil still left after separation. The threshold values of these pollutants in a produced water are usually above the permissible limit allowed by regulatory authorities for direct discharge into water bodies.

Given the quantum of the generated PW as well as the limited availability of fresh water for aquaculture and irrigated farming, there is a need for the recycling of produced water for use as process water in chemical industries as well as for the possible use in agricultural irrigation. This requires a comprehensive treatment of produced water for its safe reuse. Recycling of produced water for use in process industries is imperative because it will reduce the negative impact of these pollutants on aquatic, public health as well as promote the environmental integrity of water resources [2]. In fact, one of the foremost issues dominating discussion around the globe today is the conservation and sustainability of both surface and ground water resources [3].

In the literature, single and integrated processes have been employed to treat PW in order to reduce these pollutants to the barest minimum. Single processes adopted include ultrasound [4], advanced oxidation processes [5,6], adsorption [7] and membrane [8]. These processes involve the removal of pollutants by physical (membrane), biological and chemical means [9]. As effective as these individual processes may be, some of them are very expensive and could generate high amounts of waste products, as a result integrated processes may be an effective way to increase the effectiveness of pollutant removal as well as act as cost effective solutions for pollutant removal. Examples of integrated processes include integrated membrane process [10], adsorption and membrane [11], adsorption and photo-Fenton [12], as well as AOP and membrane processes [13] were proven effective in removal of several pollutants from PW.

A careful search of the literature reveals that a sizable number of reviews have been carried out on this subject. A review conducted by [1]

* Corresponding author.
E-mail address: b.hammadi@qu.edu.qa (B.H. Hameed).

https://doi.org/10.1016/j.jwpe.2022.103034
Received 21 March 2022; Received in revised form 26 July 2022; Accepted 27 July 2022
Available online 29 August 2022

updated information in the literature concerning chemical events and reaction mechanisms involved during the treatment of PW and the attendant consequence of the by-products on the environment. Y. Liu et al. [14] reviewed the various traditional and new treatment devices employed for the management and treatment of produced water obtained from different locations. Also, a review reported by Cabrera et al. [15] was focused on the discussion of research progress, performance evaluation of integrated biological and electrochemical approach for treatment of produced water. Another review by Yousef et al. [16] streamlined the discussion to treatment of produced water via adsorption by highlighting the challenges facing its use as a treatment method and drawing attention to other areas of future research. The review carried out by Coha et al. [5] focused the discussion on the targeted removal of organic impurities of produced water using advanced oxidation processes (AOP). To the authors' best knowledge, there is very few review articles that had the integration of advanced oxidation processes and adsorption for PW treatment as a focal point in their studies.

However, given the multi-component nature of the pollutants found in PW, no single method is adequate or unique for the comprehensive treatment of the wastewater in one step. Thus, a system integrating two or more of the aforementioned processes such as adsorption and advanced oxidation process is a welcome development. Moreover, a synergy between two or more integrated processes will provide a cost-effective approach for the treatment of PW. Thus, the objective of this review is to critically appraise and discuss the treatment of PW by adsorption and AOP and their integrated processes as reported in literature.

The main aim of this review paper was to analyze and discuss the main technologies of PW treatment using adsorption, AOP and their integrated processes. The literature search was conducted, and research papers published on the subject in 'Scopus' and 'Google Scholar' databases within the last seven years (2016–2022) were retrieved.

The keywords that were used for the search for characteristics of produced water were: "Produced Water" AND "Characteristics", "Produced Water" AND "Composition". For adsorption studies: "Produced Water" AND "adsorption" and for AOP studies: "Produced Water" AND "Advanced Oxidation Process". To search for integrated processes of adsorption and advanced oxidation: "Produced Water" AND "Integrated Process" as well as "Produced Water" AND "Hybrid System". The total number of papers reviewed was 105 papers, where 37, 31 and 5 papers were found for adsorption, AOP and integrated processes, respectively.

2. Produced water volume

The growth of the oil and gas industry over the years has resulted in the massive generation of produced water in the environment. Clark and Veil [17] reported that an estimated amount of 15 to 20 billion barrels of PW is generated annually in the United States. It is estimated that the global production of PW was 91,250 million bbl/year in 2018 [18], and is expected to increase even more with the increase in oil and gas global consumption.

Produced water generated from oil and gas extraction activities usually contains residual oil as one of the component pollutants [19]. Thus, there is a need to properly treat before releasing it to the environment in order to reduce environmental impact. Primarily, the ratio of the water to oil equivalents (WOR) or water to gas equivalents (WGR) produced from a well can range from almost zero to >50 (98 % water and 2 % oil) [20]. Moreover, 80 % of the waste and residual material generated by natural gas producing processes might be in the form of PW [21]. In addition, the source of the PW comes from the production of the fuel and could be from conventional or unconventional sources such as shale gas, coal bed methane as well as tight sand [9].

Conventional gas and oil sources originate from the geothermal forces that exert high pressures and temperatures over millions of years, causing the pyrolysis of organic material and in turn converting them to hydrocarbons in the form of petroleum, oil, and gas [22]. When this process occurs in a limited layer of porous material, an oil and gas reservoir is generated because the fuel is held in the pores of the rock. Adversely, unconventional gas and oil sources include shale gas, coal bed methane (CBM) and tight sand. Oil and gas are trapped within deep sedimentary strata in shale, requiring large volumes of water, chemicals, and energy to extract [23]. Furthermore, the matrix permeability of the shale gas is limited, and it is trapped within the shale rock, providing the gas to release. On the other hand, the tight sand has low permeability. The CBM is trapped in underground coal seams; because coal has a high surface area to volume ratio, it has the potential to allocate huge volumes of gas when compared to conventional gas resources of equivalent size [24]. The physical and chemical qualities of generated water differ significantly according to the field's geographic location, geologic formation, and hydrocarbon product type. The qualities and volume of PW change over time in a reservoir. The list of the volumes (in barrels) of the PW generated annually by various countries is listed in Table 1.

As seen in Table 1, the volume of generated PW is massive which may be attributed to expansion and growth in these countries. Thus, the management of PW has become a need. According to Nasiri et al., the management of PW may be achieved by: (1) adapting technologies to minimize PW volumes, (2) reusing or reinjecting PW back to the system to enhance recovery of oil, and (3) disposal of PW is recommended if the former is not applicable [25].

3. Characteristics of produced water

Produced water (PW) is composed of many constituents that characterize it and is part of the reason why numerous treatment processes are required to achieve the desired water quality. The major components in PW, regardless of its source, are salinity and inorganic ions, total organic carbon (TOC), organic acids, petroleum hydrocarbons including benzene, toluene, ethylbenzene and xylene (BTEX), polyaromatic hydrocarbons (PAHs) and phenols, metals, radioisotopes as well as production chemicals [20].

It was observed that total dissolved solids (TDS) values vary depending on the source and that TDS is always higher in conventional wells than unconventional wells partly due to geological variations [32]. For instance, Benko and Drewes [33] analyzed the data on the composition of PW obtained from US geological survey where 33,189 wells in western United States were considered and found that the TDS value ranged from 1000 to 400,000 mg/L. Another study undertaken by Janson et al. [34] showed that the PW sample obtained from the North Field in Qatar contained 5189 mg/L of TDS, which falls within the range obtained by [33]. According to Al-Ghouti et al. [32], the salinity of PW is much higher (around 300 parts per thousand) than of seawater, which is reported to be 32 to 36 parts per thousand. This higher salinity is caused by sodium and chloride ions dissolving from rock formations into the water. On the other hand, it is important to note that the high salinity and TDS content of this produced water may cause corrosion in pipes, which means that constant maintenance of the pipes is required. Alternatively, proper treatment of this water to reduce its salinity can aid in the reuse of this water in other areas such as reinjection into gas wells.

PW is also composed of inorganic ions existing in the form of chloride, sodium, phosphate, sulphate, calcium and hydrogen carbonate.

Table 1
Produced water of different countries.

Country	Produced water (bbl./year)	Year reported	References
USA	24,400,000,000	2017	[26]
Australia	207,570,000	2010	[27]
Iraq (Rumaila Field)	198,925,000	2013	[28]
Oman	10,331,010,000	2002	[29]
Kuwait	730,000,000	2018	[30]
Qatar	50,508,816.54	2014	[31]

According to [33] inorganic ions are released from rocks that are in contact with the formation and injected water (PW). Table 2 shows the PW chemical compositions from different sources of PW around the world. It is evident that the sodium and chloride ions are the most abundant in the PW making up 28 % and 57 % of the total composition, respectively. The results obtained by Al Haleem et al. [35] on the chloride and sodium ion concentrations were in line with those of Benko and Drewes' [33].

Other components found in PW are organic compounds and organic acids. Organic acids include the monocarboxylic and the dicarboxylic acids, of which the most abundant are formic and acetic acid [20]. Organic compounds include aliphatic and aromatic hydrocarbons and petroleum hydrocarbons. Oil and grease are also a significant component in PW either in the form of emulsion, or soluble in the water. Oil emulsions are generally more difficult to remove than oil droplets (Fig. 1). According to the work of [33], PW contains oil and grease in the range of 40 to 2000 mg/L. Moreover, the values obtained from the Rumaila oilfield in Iraq [35], north field in Qatar [34], and worldwide composition [36,37] were 654 mg/L, 47 mg/L and 275 mg/L, respectively. These values fall within the same range proposed by Benko and Drews [33], however, it is significant that the oil and grease content was the least in Qatar's North Field.

Total suspended solids (TSS), TOC and total nitrogen (TN) are also important components that make up PW. TSS include floating particles, silt, sediment, sand, algae and plankton, and concentrations range from 1.2 to 1000 mg/L [38]. TOC composition in PW was 1700 mg/L [38], and other sources report concentrations of 491 mg/L [34] and 564 mg/L [39]. TN is the sum of all nitrogen components in the produced water. Reports suggest that NO_3^- is found in the highest concentration of 2.71 mg/L in gas wells, and the highest concentration in oil wells is for NH_3 and NH_4 with concentration of 92 mg/L [39,40].

BTEX and phenols are also important components in oilfield PW. BTEX are benzene, toluene, ethyl benzene and xylene components which are volatile aromatic compounds from the oil or gas in the well. The most abundant compound is benzene ranging from 0.44 to 2.8 mg/L in the Gulf of Mexico [39]. Moreover, the BTEX concentration in produced water from oilfield reserves is around 35 mg/L [36,37] which is higher than the value obtained from Al-Ghouti et al. Phenols are aromatic organic compounds with hydroxyl functional group attached to it. The highest concentration of phenol was found in production facilities of gas condensates [32].

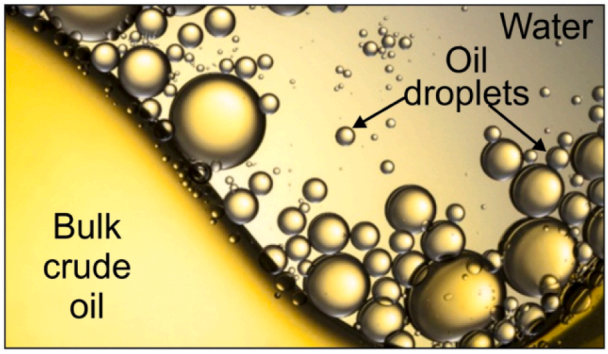

Fig. 1. Image of water-in-oil emulsion in oil. Breaking such emulsions to effectively remove water from crude oil is challenging [4].

Metals are also considered a major component in PW and the most abundant are mercury, zinc, barium, manganese and iron [9]. Concentrations of these heavy metals can range from a few ppm's to a thousand ppm in PW as demonstrated in Table 3. Heavy metals are considered toxic and carcinogenic substances and thus, their removal is mandatory due to their harmful effects on humans and biota [41].

Other chemical additives may be used during the oil and gas extraction processes such as corrosion inhibitors, scale inhibitors and gas hydrate inhibitors. The addition of these chemicals to PW is determined by manufacturers by analyzing the well and hydrocarbon type and characteristics [9]. These chemicals can also contribute to the characteristics of PW and can also negatively affect the environment when disposed of [20].

The components that majorly contribute to the characteristics of

Table 2
Produced water compositions range based on different oil production fields around the world.

Parameter	Range of values (based on comparison worldwide)	Mean value	Standard deviation	References
pH	4.3–7.45	6.30	1.23	[34,38,39,42,43]
BOD (mg/L)	750–957	853.50	146.37	[38,39]
COD (mg/L)	1220–1910	1459.13	355.24	[34,38,43]
TOC (mg/L)	491–1700	876.25	559.89	[33,34,39]
TN (mg/L)	34–647	340.50	433.46	[34,42]
TKN (mg/L)	83–155	119.00	50.91	[38,39]
BTEX (mg/L)	12.415–83.611	37.91	39.67	[33,38]
Phenol (mg/L)	11.5045–1000.001	505.75	698.97	[38]
Oil and grease (mg/L)	40.5–654	299.92	259.39	[33–35,38,42]
TSS (mg/L)	500.6–7820	2455.30	3584.21	[33,38,42]
TPH (mg/L)	45.00	45.00	0.00	[34]
Conductivity (μS/cm)	7200–87,542	48,979.33	40,228.06	[34,39,42]
TDS (mg/L)	5189–400,000	175,752.90	169,361.63	[33,34,42]
Salinity (mg/L)	7165–100,000	78,399.33	63,263.02	[39,42,43]
Chloride (mg/L)	2265–250,000	92,666.97	84,113.54	[33–35,38,42,43]
Sodium (mg/L)	1030–150,000	60,132.00	57,749.60	[33–35,38,43]
Calcium (mg/L)	329–74,000	21,929.57	26,633.70	[33–35,38,42,44]
Sulfide (mg/L)	828.00	828.00	0.00	[34]
Magnesium (mg/L)	4.7943–12,341	3164.21	4702.91	[34,35,38,42,44]
Bromide (mg/L)	51.00	51.00	0.00	[34]
Bicarbonate (mg/L)	144.4176–15,000	6563.18	7732.82	[33,35,38,42]
Sulfate (mg/L)	54–15,000	3969.37	6123.95	[33–35,38,42]
Potassium (mg/L)	44–2162	1194.50	1127.12	[34,35,38]
Thiosulfate (mg/L)	14.00	14.00	0.00	[34]
Acetate (mg/L)	347.00	347.00	0.00	[34]
Ammonium (mg/L)	11–14.54	12.77	2.50	[34,42]
Ammonia (mg/L)	9.66–74	41.83	45.50	[39,42]
Nitrate (mg/L)	2.15–9.492	5.82	5.19	[39,42]
Nitrite (mg/L)	0.05	0.05	0.00	[39]
Total phosphorous (mg/L)	0.71	0.71	0.00	[39]

Table 3
Concentrations of different metals in produced water based on oil production fields around the world.

Metal	Concentration range (mg/L)	Mean value (mg/L)	Standard deviation	References
Barium	0.058–850	362.9416	314.78	[33,35,38,44]
Strontium	500.01–6250	2619.7525	2707.43	[33,35,38]
Cadmium	0.0105–26.2	8.7710	15.09	[35,38,44]
Chromium	0.1963–97.2	24.6268	48.38	[35,38,44]
Copper	0.0613–89	29.9374	51.15	[35,38,44
Lead	0.1340–205.8	71.5787	116.32	[35,38,44]
Nickel	0.0977–162	81.0488	114.48	[35,44]
Zinc	0.255–113.4	29.7638	47.55	[35,38,43,44]
Iron	0.7133–550.05	172.2858	254.38	[38,42,44]
Manganese	0.0713–87.502	58.3584	50.48	[38,44]
Arsenic	0.1525–5.2387	3.6307	3.02	[38,44]
Boron	1.8873–50	33.9624	27.78	[38,44]
Tin	0.68	0.6797	0.00	[44]
Aluminum	205.2–360	282.6000	109.46	[38]
Lithium	26.5–32.019	29.2595	3.90	
Titanium	0.36	0.3550	0.00	
Mercury	0.0015	0.0015	0.00	

produced water are inorganic and organic ions, organic acids, salinity and TDS (and conductivity), metals, hydrocarbons such as BTEX and phenols, oil and grease as well as chemical additives. Observations by Al Haleem et al.'s team [35] documented that the PW was responsible for scale formation, corrosion, bacterial growth as well as foul equipment in the Rumaila facility. Therefore, suitable treatment of the produced water is required to ensure that equipment is not damaged, and that the effectiveness of these equipment is not diminished by scale and hydrate formations. Moreover, different water treatment technologies are required depending on the purpose of reuse and the source characteristics of PW.

4. Adsorption process

Adsorption is one of the most effective methods when compared to other physical and chemical produced water (PW) treatment methods [45]. Owing to the increasing amount of PW being generated worldwide, adsorption is a cost-effective treatment method to treat large volumes of PW with diverse contaminants [16]. Another advantage of the adsorption process is the ability for regeneration of adsorbent, which can be achieved through thermal regeneration or the use of chemical eluents to aid in the desorption process. This signifies the importance of adsorption methods in the oil and gas industry. Table 4 summarises the adsorbents discussed below, their performance as well as information regarding the kinetic and isotherm parameters.

4.1. Removing COD, DOC and TOC content

Residual biomass can make an excellent adsorbent as demonstrated by Gallo-Cordova et al. [46], where the performance of walnut shell adsorbent for the removal of organic content from real PW was compared with other residual biomass such as palm shell, sawdust, cocoa beans, orange, banana and passion fruit peels. The only biomass adsorbents that were able to remove organic compounds were walnut shell, palm shell and sawdust with chemical oxygen demand (COD) removals of 4.9 mg/g, 5.6 mg/g, and 33 mg/g, respectively. The higher adsorption capacity of sawdust was attributed to the lower organic total solids (OTS) percentage. However, the other residual biomass displayed an increase in COD, which indicates that these are not suitable [46]. In another study, waste sawdust (WS) was used as adsorbent to treat PW samples from an oilfield in Iraq with an initial concentration of organic content of 130 mg/L [47]. The maximum adsorption capacity of 23.97 mg/g was obtained at the optimum conditions of pH 3, 2 g dosage, 90 min contact time, and particle size of 0.075 mm. Comparison of the two WS adsorbents obtained by [46] were much better in terms of adsorption capacity, which was due to higher initial COD concentration, which facilitated a greater number of COD adsorbed by the WS. However, one drawback of using WS as an adsorbent is the ability to compress inside a column, and therefore, suitable procedure should be established to maximise the use of such adsorbent in continuous operation.

Treatment of COD in PW obtained from Al Ahdab oil field in Iraq using moringa husks (MH) and activated moringa husks (AMH) as adsorbent gave a maximum adsorption uptake of 22.8 mg/g and 26.88 mg/g respectively [48,49]. The higher adsorption uptake of AMH compared to MH is due to a greater specific surface area (913 m^2/g for AMH and 713 m^2/g for MH), since the functional groups present in both MH and AMH are the same. From FTIR, the functional groups most prominent and that aided in the adsorption process were hydroxyl (-OH), amine ($-NH_2$) and carboxyl groups (-CO) [48,49].

Biochar – a carbon rich material- could be utilized for the effective treatment of real PW. Tea waste biochar (TWBC) and modified tea waste biochar (MTWBC) were reported for the removal of organic compounds from PW with an initial COD concentration of 2400 mg/L [50]. The maximum adsorption of COD was 12 mg/g at pH of 12, dosage of 250 mg/L, contact time of 120 min for TWBC. For MTWBC, the optimal capacity (21.74 mg/g) was obtained at a dosage of 250 mg/L, pH 3, contact time of 180 min MTWBC exhibited better performance due to large surface area (82 m^2/g) and pore volume (0.08 cm^3/g) compared to TWBC (60 m^2/g and 0.02 cm^3/g), as well as more functional groups (such as carboxyl groups) that facilitated the adsorption of organic content [50]. Biochar was also utilized in the adsorption of dissolved organic content (DOC) in shale gas flowback and PW (SGFPW) from Sichuan Basin (25.07 mg/L) in a batch experiment in the form of porous biochar aerogel (PBA) tuned by 11.5 wt% KOH and 12.0 wt% Urea (PBA-$A^{11.5}U^{12.0}$) [14]. The reported maximum capacity (205.86 mg/g) was obtained at an adsorbent dosage of 300 mg/L, 30 min contact time, temperature of 25 °C without adjusting the pH. The cost of PBA-$A^{11.5}U^{12.0}$ adsorbent was 3.08 RMB/g, which was found to be less than of other adsorbents, suggesting that PBA-$A^{11.5}U^{12.0}$ can be used in the field for DOC adsorption as a cost-effective and efficient adsorbent [14]. It is evident that PBA-$A^{11.5}U^{12.0}$ had superb removal of organic content in juxtaposition to TWBC and MTWBC, not only due to the higher capacity of adsorbed organic content, but also due to its quick time to reach equilibrium, which would be beneficial to use on an industrial scale.

Adewoye et al. [51] synthesized multiwalled carbon nanotubes (MWCNTs) purified with H_2SO_4/HNO_3, then functionalized with 1-pyrenebutanoic acid N-hydroxyl succinimidyl ester (PSE) to produce functionalized multiwalled carbon nanotubes (FMWCNTs) for the removal of TOC. BET characterization revealed that the FMWCNTs surface area of 831.80 m^2/g was greater than MWCNTs and purified MWCNTs (PWCNTs). The PW was supplied from an oil exploration company in the Niger Delta, with an initial TOC concentration of 55.53 mg/L. The TOC removals % were 79.2 % and 93.6 % for PMWCNTs and FMWCNTs, respectively. Using central composite design (CCD), the maximum adsorption capacity was 260 mg/g at the optimal conditions of 49.70 min contact time, temperature of 34.81 °C, and a dosage of 0.02 g. FMWCNTs exhibited excellent efficiencies compared to MWCNTs and PMWCNTs, in addition to exhibiting the highest adsorption capacity for TOC which is attributed to its high surface area [51]. In order to further evaluate the effectiveness of FMWCNTs as adsorbents, reusability studies and column studies should be performed since it has great potential in TOC removal.

4.2. Removal of oil content and hydrocarbon-based compounds

Carbon-based materials can make excellent adsorbents for emulsified oil from PW. Fathy et al. [45] synthesized amorphous carbon thin film (ACTF) adsorbent using oil palm leaves for removal of emulsified condensate oil in synthetic PW. The reported ACTF had high surface area (450.57 m^2/g) and porosity (0.009 cm^3/g) as well as numerous thin

Table 4
Summary of the literature on the adsorption isotherms and kinetics parameters for different adsorbents.

Adsorbent	Pollutant	Experimental conditions	Type of PW	q_{max} (mg/g)	Isotherm model	Kinetic model	Reference
Walnut shell	COD	T = 25 °C, D = 0–10 g/40 mL, t = 1–120 min, COD_i = 300–1400 mg/L	Real	4.9	Langmuir	PFO	[47]
Palm shell	COD			5.6	Langmuir	PFO	
Sawdust	COD			33	Langmuir	PFO	
ACTF (amorphous carbon thin film)	Emulsified condensate oil	**Batch:** t = 0.5–24 h, C_0 = 100–2500 mg/L, T = 288–318 K, D = 5 g in 25 mL **Fixed-bed:** Flow = 2.2–8.4 mL/min, h = 5–15 mm	Synthetic	132.77	Langmuir		[46]
Graphene nanoplatelets	Emulsified oil	**Batch:** D = 1–7 g/L, t = 0–120 min, [NaCl] = 0–2000 ppm, pH = 2–12, T = 25–50 °C **Fixed-bed:** h = 0.3–0.6 cm, flow = 0.4–0.8 mL/min	Synthetic	100	Freundlich	PSO	[53]
Graphene magnetite				85			
Zeolite	Ions	D = 0.3 g/50 mL, T = 25 °C, t = 4 h, pH = 2	Real (RN CE Operation unit)				[67]
Alumina (γAl_2O_3)							
LDH (lamellar double hydroxides)							
GIC (graphite intercalation compound)	Dispersed oil emulsions	C_0 = 103–276 mg/L, t = 10–20 min	Synthetic	2.2	Temkin		[54]
RR-AW (reactive red - agro waste)	Hg (II)	pH = 2–11, C_0 = 0.25–1.8 mM, T = 30–60 °C, D = 50 mg/50 mL, t = 2 days	Synthetic	2.6 mmol/g	Langmuir	PSO	[71]
	MeHg(II)			0.76 mmol/g	Temkin		
H_2TiO_3	Lithium	T = 30 °C, D = 0.01–0.2 g, V = 10 mL, t = 24 h, TOC = 0–200 %	Synthetic	2.14 mmol/g	Langmuir	PSO	[65]
Optipore L493	Emulsified oil	V = 50 mL, T = room temp., D = 0.125–2 g, t = 15–1440 min, pH = 2–10, C_0 = 3–27 mg/L	Synthetic	9.51	Toth	PSO	[56]
Lewatit AF5				13.35	Dubnin-Radushkevich		
Amberlite XAD 7				11.86	Freundlich		
Amberlite IRA958						PSO	
Chemically modified kiwi peels	Oil content	V = 100 mL, T = 25 °C, D = 0.5–2 g, t = 30–120 min, pH = 2.16–9.67, C_0 = 100 ppm	Real (Al-Ahdab oilfield)	13.36	Freundlich		[59]
Cassia surattensis seeds	Oil content	D = 0.5–3 g, pH = 2–9, t = 30–150 min, 150 mL, T = 25 °C, C_0 = 118 ppm	Real (Al-Ahdab oilfield)	12.18	Freundlich		[58]
Moringa husks	Organic content	T = 25 °C, pH = 2–10, D = 0.5–2 g, C_0 = 210 ppm, t = 30–150 min	Real	22.88	Langmuir		[49]
Activated moringa husks				26.88			
Modified silica	TDS	T = 25 °C, V = 1 L, D = 0.2–0.4 g, t = 30–180 min, pH = 7, TDS_0 = 242,500 mg/L, Ec_0 = 19,300 mg/L	Real				[72]
	Ec						
Moringa peels	Organic content	C_0 = 210 ppm, T = 25 °C, pH = 2–10, D = 0.5–2 mg, t = 30–150 min	Real	22.88	Langmuir		[50]
Activated moringa peels				26.88			
Imperata cylindrica	Oil content	C_0 = 54.6 mg/L, V = 100 mL, pH = 3–9, T = 30–60 °C, D = 0.05–0.4 g, t = 15–90 min	Real (Midland Oil Company)		Langmuir	PFO	[57]
Polyurethane (PU) based algae bicomposite	Boron	C_0 = 6.44 mg/L, D = 1 g, V = 50 mL, t = 72 h, pH = 7.19, PU/algae = 1.12–1.20 g/mL	Real (Oxy-Oman site)				[68]
Fe_3O_4/Bent NC (iron oxide/bentonite nanocomposites)	Oil content	D = 0.05–0.2 g, T = 298 K, pH = 3–9, C_0 = 66–170 mg/L	Synthetic	54.05	Langmuir	PSO	[55]
CS (seed of moringa oleifera)	Oils and greases	V = 200 mL, t = 4 h, D = 0.5–3.5 g/L, T = 298–318 K	Synthetic	111.11		PSO	[62]
CV (pod of moringa oleifera)				104.17			
γ-Al_2O_3 (gamma-alumina)	Iron	C_0 = 39 ppm, t = 30–180 min, pH = 4–10, D = 0.2–0.4 mg/L, T = 25 °C	Real (Middle Oil Company)				[74]
Waste sawdust (WS)	Oil/organic content	C_0 = 130 ppm, V = 500 mL, T = 25 °C, t = 30–150 min, D = 0.5-3 g, pH = 2–10	Real	23.97	Freundlich		[48]
Macronet MN 202	Naphthenic acid (NA)	V = 50 mL, pH = 4 or 8, C_0 = 500 mg/L, salinity = 100 g/L, D = 4 mg/L, T = 50 °C, t = 24 h	Synthetic	119.695	Freundlich - BET	Intra-particle diffusion	[7]
Dowex L493				57.03	Langmuir - BET		
TWBC	COD (organic)	V = 100 mL, C_0 = 25–3000 mg/L, T = 25 °C, pH = 3–12, t = 10–360 min	Real (SE Asia)	12	Langmuir	PSO	[51]
MTWBC				21.74			
Castor oil	Oil content	V = 250 mL, T = 25 °C, D = 0.5-2 g, C_0 = 130 ppm, pH = 2–9.5, t = 30–150 min	Real	23.08	Freundlich		[60]
Modified castor oil				25.7			
AC-Fe (moringa oleifera seed and modified with iron nanoparticles)	Oils and greases	T = 298–318 K, C_0 = 100–500 mg/L, pH = 4–9, [NaCl] = 0–20 g/L, D = 2.5 g/L, t = 4 h, V = 200 mL	Synthetic	121.95	Freundlich	PSO	[63]
CH/PEG/MWCNT	Oil content	V = 25 mL, pH = 3–11, D = 1–5 g/L, C_0 = 0.2–1 g/L	Synthetic	400	Langmuir	PSO	[61]
AMB (APTES functionalized magnetic bentonite)	Ba (II)	pH = 3–9, D = 0.12–0.6 g/L, t = 15–120 min, C_0 = 25–200 mg/L, T = 30–70 °C	Synthetic	124.8	Langmuir	PSO	[69]
	Sr (II)			120			
PBA-$A^{11.5}U^{12.5}$ (PBA tuned by 11.5 wt.% KOH and 12.0 wt % urea)	Organic content (DOC)	C_0 = 300 mg/L, t = 30 min, T = room temp.	Real (Sichuan Basin, China)	205.86	Freundlich	PSO	[14]

(*continued on next page*)

Table 4 (*continued*)

Adsorbent	Pollutant	Experimental conditions	Type of PW	q_{max} (mg/g)	Isotherm model	Kinetic model	Reference
PEG/Fe_3O_4/GO-NH_2	Ca^{2+} Mg^{2+}	pH = 7.3, T = 50 °C, $[Ca^{2+}]_0$ = 3604 mg/L, D = 0.4 g, t = 10–120 min, $[Mg^{2+}]_0$ = 657.8 mg/L, V = 200 mL	Synthetic	2845.3 406.1		PSO	[70]
CAZ (activated with $ZnCl_2$) CAH (activated with H_3PO_4) CANa (activated with NaOH)	Oils and greases	V = 50 mL, C_0 = 223 mg/L, D = 100 mg, T = 25 °C	Real	 294.41	Freundlich Langmuir	PSO	[64]
FMWCNT (functionalized multi walled carbon nanotubes)	Total organic carbon (TOC)	T = 30–50 °C, V = 100 mL, D = 0.02–0.1 g, t = 10–60 min	Real	256.9	Harkins-Jura	PSO	[52]
Walnut shell	^{226}Ra	**Batch:** D = 100 g/L, particle size = 300-425 μm, [^{226}Ra] = 420 Bq/L, t = 15–360 min, pH = 1.5–10, T = 15–60 °C **Fixed-bed:** h = 5–15 cm, [^{226}Ra] = 700 Bq/L, flow = 4–10 mL/min	Real	19 (Bq/L)	Freundlich Langmuir		[73]
HMO-2 (manganese based lithium adsorbent Li:Mn = 2:1)	Lithium ions	T = 70 °C, D = 2 g/L, t = 30 min	Real (Duvernay Foundation, Canada)	18			[66]
HMO-3 (manganese based lithium adsorbent Li:Mn = 3:1)				27			

KEY: D: dosage of adsorbent, T: temperature, t: time, h: bed height, C_0: initial concentration of pollutant, V: volume of PW.

mesopores needed for trapping and adsorption of the emulsified oil. The maximum capacity for ACTF is 132.77 mg/g at optimum conditions of 308 K, time of 6 h, and an initial concentration of 1000 mg/L of oil in PW. Another study reported by Abou Chacra et al. [52] investigated graphene nanoplatelets for the removal of emulsified heavy crude oil in synthetic PW in both batch and fixed bed systems. The best adsorption conditions for graphene (100 mg/g) were at dosage of 3 g/L, contact time of 60 min, pH of 10, salinity of 1500 ppm and 25 °C. Graphite intercalation compound (GIC) adsorbent was investigated by Fallah and Roberts [53] in a batch experiment at conditions using PW with initial oil (n-heptane) concentration of 103 mg/L, and real PW with initial concentration of 152 mg/L. Experimental conditions (batch) were at pH of 4.5, a temperature of 22 ± 3 °C, contact time of 30 min, adsorbent dosage of 20 g. It was reported that the maximum adsorption capacity of 2.2 mg/g was achieved in 30 min and the oil removal efficiency reduced from 100 % to 87 % after five cycles. The rapid kinetics of the adsorption and the lower adsorption capacity were mainly attributed to the non-porous structure of the GIC. However, this non-porous structure allows for faster and lower-energy consuming regeneration using electrochemical processes [53]. It is evident that GIC has the poorest performance when compared with other carbon-based adsorbents [45,52], despite having the lowest equilibrium time and fastest kinetics.

It is evident according to literature that iron-based adsorbents can effectively adsorb emulsified oil from PW. The magnetic property that some of the iron-based materials acquire, gives them an added ability to reclaim magnetic materials. Abou Chacra et al. [52] integrated magnetite into graphene nanoparticles and discovered that the optimal adsorption (85 mg/g) by graphene magnetite occurred at a dosage of 4 g/L, contact time of 30 min, pH of 3.5, salinity at 1000 ppm and 25 °C. In addition, graphene magnetite could be regenerated using n-hexane and re-used with no changes in efficiency in both processes. Iron oxide/bentonite nanocomposite (Fe_3O_2/Bent NC) material was synthesized by Ewis et al. [54] and applied for emulsified diesel oil (100 ppm) removal from synthetic PW in a batch process. The adsorption capacity and percentage removal of 54.05 mg/g and 67 %, respectively were obtained at the optimum conditions of 90 min, 0.1 g of adsorbent, and pH 6.5 [54]. It was evident that graphene magnetite showed better performance in terms of both adsorption capacity as well as adsorption kinetic. It is worth noting that upon integrating iron-based particles in the adsorbent, its adsorption capacity declines.

In an attempt to study the performance of polymeric resins, Albatrni et al. [55] investigated four commercial polymeric resins (Optipore L493, Amberlite IRA 958, Amberlite XAD 7 and Lewatit AF5) for the removal of emulsified oil from synthetic PW with an initial oil concentration of 20–50 mg/L oil. The oil used is composed of hydrocarbon of low molecular weight gasoline, and a surfactant was added to produce the emulsions. The equilibrium times were 1 h, 4 h, and 8 h for XAD7, IRA 958, and both L493 and AF5, respectively. The % removal of 96.3 %, 96.5 %, and 97.5 % were reported at the optimum dosages of 0.5 g, 1.5 g, 0.75 g, and 0.375 g for XAD 7, L493, AF5 and IRA 958, respectively at room temperature, and an optimum pH of 6.7. The adsorption capacities of the resins in removing oil emulsions were 11.86 mg/g, 9.51 mg/g and 13.35 mg/g for XAD7, L493 and AF5, respectively [55]. The percentage removal of IRA 958 was poor and therefore not reported in the study, however, it would have been good to add them for purpose of comparison. The resins used were commercial resins, so it would be beneficial to investigate modified forms of these resins to see if their capacities would be enhanced or not as well as their performance after regeneration.

Biosorbents were reported for the removal of oil from PW. Alatabe et al. [56] employed Taguchi method to statistically optimize conditions for the oil (n-hexane) removal (54.6 mg/L) from real PW using *Imperata cylindrica*. 97 % oil removal was achieved at a temperature of 30 °C, pH of 9, dosage of 0.1 g per 100 mL PW, and a contact time of 90 min. Moreover, *Cassia surattensis* seeds were investigated by [57] for adsorption of oil (crude oil) (118 ppm) from real PW. *Cassia surattensis* seed's adsorption capacity of 12.18 mg/g was obtained at an optimal pH of 2, contact time of 120 min and dosage of 2 g in 150 mL of PW at a temperature of 25 °C (±3 °C) and agitation speed of 200 rpm.

In the study reported by Saleh Jafer and Hassan [58] for the adsorption of oil (110 mg/L) by chemically modified kiwi peels, the maximum capacity was 3.36 mg/g at the optimum condition of 150 min, pH of 2.16 and dosage of 1.5 g in 100 mL of real PW from Al-Ahdab oilfield at 25 °C. Hassan et al. [59] reported the use of castor oil and modified castor oil for treatment of real PW with oil content of 130 ppm by batch adsorption. The adsorption capacities acquired by castor oil and modified castor oil were 23.08 mg/g and 25.7 mg/g, respectively at pH of 2, 1.5 g adsorbent dosage, 120 min and temperature of 25 °C. It was reported that the enhanced capacity of the modified castor oil compared to castor oil was due to the anionic character of the oil, and in comparison, with the modified kiwi peels, the castor oil was a better oil adsorbent due to the anionic charge on the surface of the modified castor oil.

The removal of oil (crude oil) (1000 mg/L) from synthetic PW by adsorption using composite materials such as biodegradable polymer of chitosan; chitosan/polyethylene glycol/multiwalled carbon nanotubes

(CH/PEG/MWCNT) was studied by Mottaghi et al. [60]. The CH/PEG/MWCNT adsorption capacity of 400 mg/g was achieved at pH 3, adsorbent dosage of 1 g/L, and ratio of chitosan to polyethylene glycol of 3:1. Chemisorption was reported as the main mechanism due to discovery of covalent bonds between adsorbent and adsorbate. CH/PEG/MWCNT regeneration using n-hexane yielded an insignificant decrease in oil capacity as well as negligible weight loss of the adsorbent after 5 cycles as illustrated in Fig. 2 [60].

The synthesis of an adsorbent from moringa oleifera seeds (CS) for removal of oils and greases (sourced from crude oil) from synthetic PW with a total oil and grease (TOG) of 300 mg/L was reported by Santos et al. [61]. CS synthesized had an adsorption capacity and percentage removal of 111.11 mg/g and 87.2 %, respectively at 298 K. Menezes Santos et al. [62] modified the moringa oleifera seeds with iron nanoparticles (AC-Fe) for synthetic PW treatment of oil and grease (300 mg/L). The AC-Fe maximum capacity for oil and grease content (OGC) was 121.95 mg/g which corresponded to 94.3 % OGC removal. It can be observed that the modification with iron nanoparticles (AC-Fe) enhances the adsorption of oils and greases compared to CS, this is attributed to the greater surface area (578.4 m^2/g) and porosity (0.48 cm^3/g) of AC-Fe.

Moringa oleifera pods (CV) were also utilized for the removal of oils and greases (TOG = 300 mg/L) from synthetic PW [61]. The high adsorption capacity of CS (111.11 mg/g) compared to CV which reached 104.17 mg/g, is justified since CS (0.16 cm^3/g) exhibits much greater pore volume than CV (0.06 cm^3/g). Chemically modified moringa oleifera pod was also reported for the removal of oil and grease from real PW in batch process [63]. The adsorption capacity of 294.41 mg/g (95 % removal) is observed for the adsorbent modified with phosphoric acid (CAH). The percentage removal is higher than that achieved for the zinc chloride modified sample (CAZ) (93 %) and sodium hydroxide (CANa) (60 %). The outstanding performance of CAH was attributed to well-developed pore structure caused by the acid activating agent [63]. This suggests that modification of the moringa oleifera with chemical reagents is effective in increasing the capacity of the CV.

4.3. Removal of metal ions and toxic metals

Jang and Chung [64] studied the removal of lithium ions from synthetic PW using H_2TiO_3 adsorbent. The experiment was done at a temperature of 30 °C, a dosage of 0.03 g of adsorbent into 10 mL of the PW for 48 h. The adsorption capacity of H_2TiO_3 was 2.14 mmol/g (14.85 mg/g). It was also reported that as the TOC content increased, the amount of lithium adsorbed decreased due to the competition of TOG with lithium ions on the surface [64]. The adsorption of lithium from flowback produced water (FPW) from Duvernay Formation in Canada was also investigated by using manganese-based lithium adsorbents with ratios of Li: Mn of 2:1 (HMO-2) and 3:1 (HMO-3) [65]. The optimal

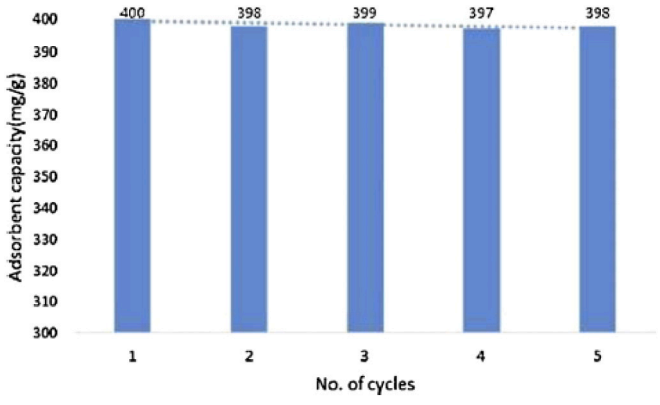

Fig. 2. Cyclic oil adsorption on CH/PEG/MWCNTs hydrogel during regeneration process [60].

adsorption capacities of 18 mg/g (HMO-2) and 27 mg/g (HMO-3) were reported at a temperature of 70 °C, adsorbent dosage of 2 g/L, 30 min, and a pH 8. The desorption of lithium from HMO-2 and HMO-3 adsorbents was performed using 0.5 M H_2SO_4 where all the lithium adsorbed was desorbed in 5 min. It is apparent that HMO-3 had the best adsorption potential compared to both HMO-2 as well as the H_2TiO_3 adsorbents, despite operating at higher temperature (70 °C). This can be disadvantageous when implementing on a large scale due to the increased energy requirements, which could drive operational costs up.

The attempt of removal of cations and anions from real PW sampled from an operation unit in Brazil was studied using three adsorbents: zeolite, alumina and lamellar double hydroxides (LDH) [66]. Ions that were analyzed were: chloride, formate, bromide, sulfate, sodium, ammonia, potassium, calcium, magnesium, strontium, barium, iron, cadmium, chromium, manganese, nickel, arsenic, silver, boron, beryllium, cobalt, phosphorous and lead ions. It was observed that LDH preferably removes anions, zeolites preferably remove cations, while alumina can remove both cations and anions. The best removal capacities were reported by alumina at a pH 2, contact time of 4 h, dosage of 0.30 g of adsorbent in 50 mL PW. This is due to its superior surface area (250 m^2/g) compared to zeolites (5 m^2/g) and LDH (12 m^2/g) [66] which allowed for more ions to be adsorbed on the surface. The optimal adsorption capacity of the three adsorbents was not reported and therefore it was difficult to see how these adsorbents perform in the conditions reported.

Polyurethane (PU) based algae bio composite material was investigated for the removal of boron (6.44 mg/L) from real PW from Oxy-Oman site [67]. The PU bio composite was able to remove 84–75 % of boron in PW, however the process was very slow as it took 72 h to be complete at a pH 7.19, dosage of 1 g/ 50 mL of PW. Boron removal was at the maximum value when no filler material (algae) was added [67], since more vacant sites are available for boron to be adsorbed onto.

Nanocomposite materials could be beneficial in the adsorption of barium (52 ppm) and strontium (103 ppm) ions from synthetic PW, nanocomposite 3-aminopropyltriethoxysilane functionalized magnetic bentonite (AMB) was investigated by El Maghrabi et al. [68]. Adsorption capacities of 124.8 mg/g and 120.0 mg/g were achieved for Ba^{2+} and Sr^{2+} ions, respectively, at pH 9, 60 min contact time, dosage of 0.4 g/L, at 25 °C. The adsorption process relied heavily on pH and was considered a control parameter in the adsorption process. AMB was regenerated by eluting it with HCl, and after three cycles there was no substantial decrease in adsorption capacities for both ions [68]. In a study by L.He et al. [69] another nano adsorbent PEG/Fe_3O_4/GO-NH_2 was investigated (Fig. 3) for the removal of Ca^{2+} (3604 mg/L) and Mg^{2+} (657.9 mg/L) ions from synthetic PW. The adsorption capacity of the PEG/Fe_3O_4/GO-NH_2 was found to be 2845.3 mg/g of Ca^{2+} and 406.1 mg/g for Mg^{2+} at pH 7.3 and 50 °C The PEG/Fe_3O_4/GO-NH_2 was regenerated for five cycles. Core displacement experiments indicated that after treatment using PEG/Fe_3O_4/GO-NH_2, the oil recovery was improved by 11.8 %. This shows the effectiveness of PEG/Fe_3O_4/GO-NH_2 for Ca^{2+} and Mg^{2+} removal and post use in oil recovery [69]. It can be realized that PEG/Fe_3O_4/GO-NH_2 had a greater di-valent anions adsorption capacities, however it can be observed that the operational temperature is high and could result in a greater operational cost.

The removal of heavy metals such as inorganic mercury Hg (II) and organic methyl mercury MeHg(II) ions from synthetic PW using reactive red agrowaste adsorbent (RR-AW) was reported by [70]. RR-AW could adsorb 2.60 mmol/g of Hg (II) and 0.76 mmol/g MeHg(II) from PW at 30 °C, dosage of 50 mg adsorbent in 50 mL PW, contact time of two days and a pH 5. Regeneration of RR-AW was also investigated, where the efficiency of the adsorbent was not affected as the number of cycles increased. Selectivity studies also showed that using the RR-AW adsorbent in oilfield PW has the affinity to remove Zn and Hg ions, this shows that RR-AW adsorbent can also be used in other PW treatment applications. Another heavy metal, iron (39 ppm) was removed from PW obtained from Middle Oil Company in Iraq using Gamma-alumina

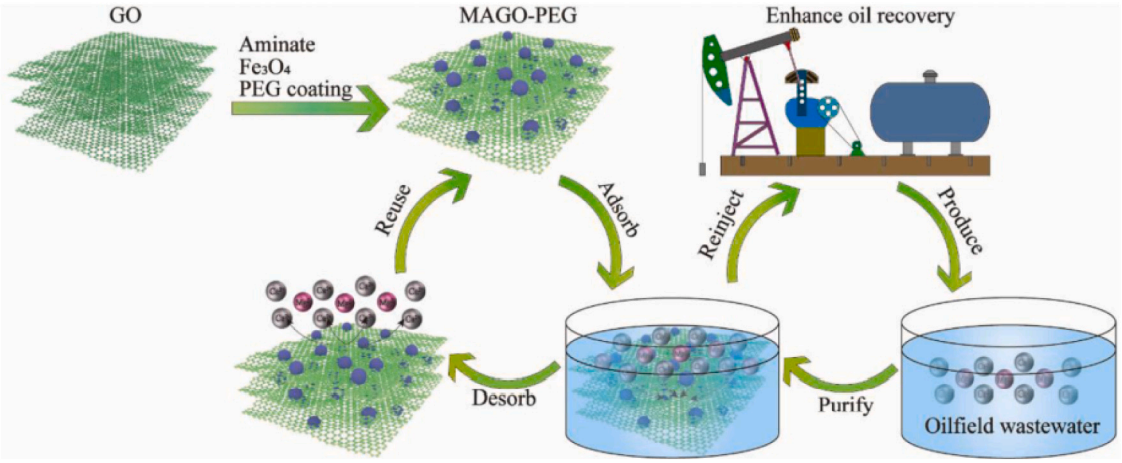

Fig. 3. Schematic diagram of the preparation and application of PEG/Fe_3O_4/GO-NH_2 [69].

(γ-Al_2O_3) adsorbent synthesized by [71]. The maximum recovery of the iron ions of 99.9 % achieved at optimal pH 7, 90 min contact time and 0.4 mg adsorbent dosage indicated that γ-Al_2O_3 is an effective adsorbent for this purpose.

Al Masri et al. [72] studied the use of walnut shell as an adsorbent for ^{226}Ra ions removal from real PW. The adsorption capacity of walnut shell is 19 Bq/g in batch operations and 10.1 Bq/g in column operation. Walnut shell was desorbed using 0.5 mol/L of NaCl solution acidified with 37 % HCl at a temperature of 60 °C for 3 h which was able to remove 31.3 % of ^{226}Ra and requires three washings in order to achieve complete desorption of ^{226}Ra. This shows the capability of walnut shell to remove vital pollutants such as radioactive materials.

4.4. Removal of other compounds

A comparison between electrocoagulation and adsorption as treatment processes were conducted by [73] for the removal of TDS (242,500 mg/L) and electrical conductivity (Ec) (19,300 µS/cm) from PW obtained from East Baghdad oilfield in Iraq. The adsorbent used in the study was modified silica. The lowest possible TDS and Ec values attained after the adsorption treatment were 513 mg/L and 781 µS/cm at 25 °C, an adsorbent dosage of 0.4 mg/L, pH 7 and 180 min, while electrocoagulation failed to reduce TDS and electrical conductivity [73]. On another note, Hendges et al. [7] studied and evaluated 13 different commercial adsorbents for the removal of naphthenic acids (NAs) from synthetic PW with initially 500 mg/L of NA. MN 202 (119.659 mg/g)

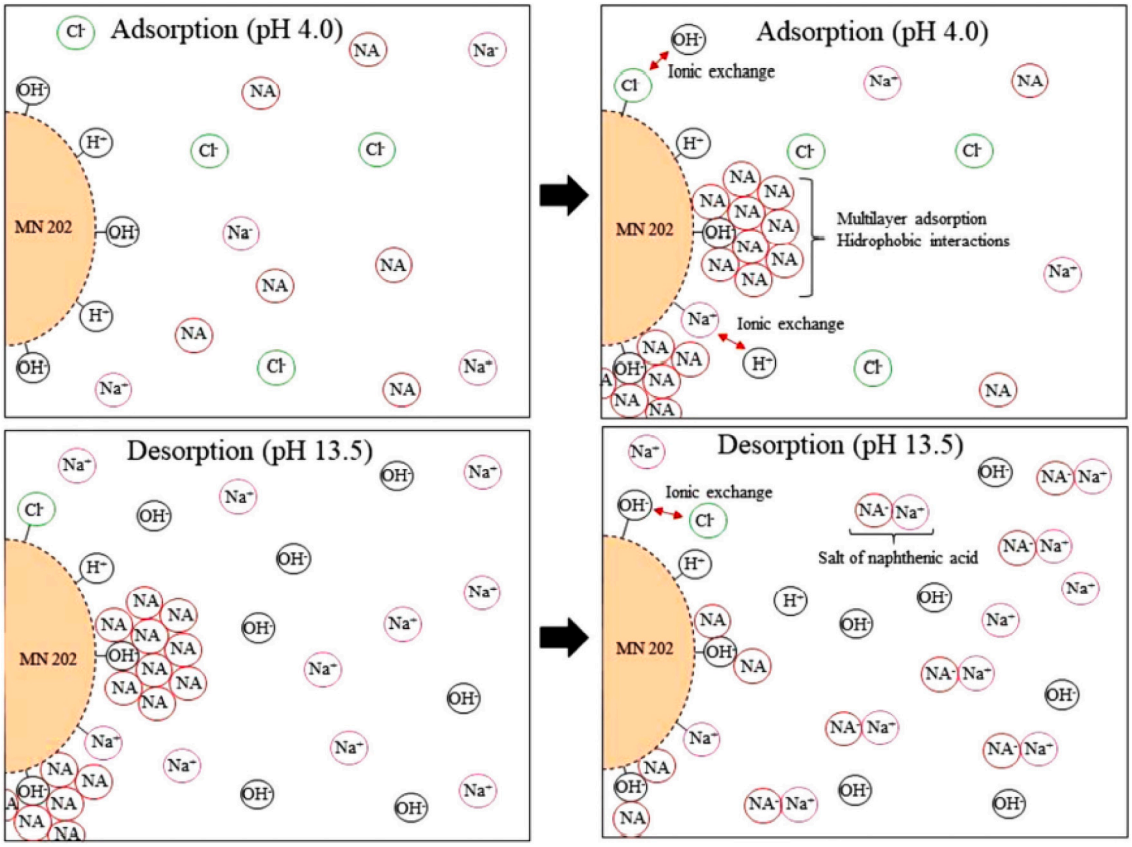

Fig. 4. Schematic diagram for adsorption and desorption of NA on MN 202 [7].

and L493 (57.030 mg/g) obtained the best adsorption capacities at a 50 °C, pH 4, dosage of 4 mg/L and 24 h. The MN 202 capacity was greater than of L493 despite having a greater surface area, the better adsorption capacity was attributed to the greater pore size, which indicates a greater adsorption of NA. Desorption of adsorbents was also investigated using a basic solution, where complete regeneration could be achieved at pH 4, NA initial concentration of 200 mg/L, and 25 °C. The mechanism of NA removal, as demonstrated in Fig. 4, was found to be dependent mainly on hydrophobic ion exchange and electron repulsion [7]. The former indicates the wide applicability of adsorbents in the removal of many pollutants, and therefore suggests the viability and importance of the development of adsorbents.

4.5. Effect of experimental conditions in batch adsorption

4.5.1. Effect of initial concentration and contact time

Since adsorption is a mass transfer phenomenon, initial concentration of the pollutants is crucial since it influences the driving force of pollutants from the solution and on to the adsorption site. In the removal of oil from PW using graphene intercalation compound (GIC) adsorbent [53], it was reported that as the initial oil concentration was decreased from 276 mg/L to 103 mg/L, the oil removal percentage was decreased from 96 % to 84.6 %. Since this process heavily depended on the external mass transfer, the trend can be justified, since an increase in the initial concentration of the oil acts as a driving force for the pollutant to be adsorbed on the surface.

Adversely, in the study by Ewis et al. [54] for the removal of emulsified oil from PW on Fe_3O_2/Bent NC, the initial oil concentration and the removal percentage seemed to have an inverse relationship, as the concentration of the oil increases, the percentage of pollutant removed decreases. In another study for the removal of OGC using AC-Fe adsorbent, as the initial oil concentration increases, the higher the adsorbed capacity of AC-Fe, however, it is to be considered that an exceeded amount of OGC can clog the active sites [62].

The contact time refers to the time in which the adsorbent is in contact with the PW sample in batch adsorption experiments and is considered a vital parameter affecting the adsorption process. The dominating trend that was exhibited by all studies was that as the contact time between the adsorbent and the solution increased, the capacity of the adsorbent increased rapidly in the beginning. However, after some time, the adsorbent becomes saturated, and the capacity reaches a plateau. This was evident when *Cassia surattensis* seeds were investigated for the removal of oil from PW [57]. The equilibrium time reached by the batch adsorption was 2.5 h. In the first 30 min, the adsorption process was rapid since there are more vacant spaces for adsorption, and as the time increases, the adsorption decelerates since the vacant spots are filled and the organics are dispersed.

4.5.2. Effect of adsorbent dosage

Adsorbent dosage is an important factor in the adsorption processes and found to influence the adsorption process significantly. The main trend that most of the literature abides by is the fact that the adsorption capacity and dosage are directly proportional. This suggests that as the dosage increased, the adsorption capacity also increased. This was demonstrated in the study of J. et al. [48], where changing the dosage from 0.5 to 2 mg resulted in increase in the adsorption capacity of organic content, which in result increased the removal percentages from 40.2 % to 54.5 % in moringa husks (MH) and from 44.5 % to 64 % in activated moringa husks (AMH). Moreover, in the study of the removal of oil using Fe_3O_2/Bent NC adsorbent reported by [54], the change in adsorbent dosage from 0.05 g to 0.1 g enhanced the percentage oil removal from 18 % to 28.4 %. Similar results were obtained using walnut shell's adsorption of organic content [47], since an increase in dosage from 0.5 g to 3 g, the oil recovery percentage increased from 39.6 % to 62.3 %. These trends can be justified since increasing the dosage corresponds to more available adsorption active sites and hence increases the amount of adsorbed pollutant [47,48,54].

However, other studies have reported contradicting results to the former discussed trends, as the adsorbent dosage increases, the adsorption capacity decreases. For instance, for the two adsorbents tea waste biochar (TWBC) and modified tea waste biochar (MTWBC) used for COD removal from PW [50], when the biochar dosages were varied from 25 to 3000 mg/L, the optimum dosage was reported as 250 mg/L and increasing dosage beyond this value decreased COD removal. This was attributed to three reasons: (1) saturation of the adsorbent surface, (2) agglomeration of adsorbent at higher dosages, and (3) the electrostatic repulsion between the adsorbate and the functional groups presents on the adsorbent surface [50]. Another study by Mottaghi et al. [60] revealed that as the CH/PEG/MWCNT dosage decreased and the oil concentration increased, the adsorption capacity reached its highest. This is because of the increased amount of adsorption sites that are unsaturated when dosage increases [60]. The removal of TOC using FMWCNT [51] had a similar behavior, as the FMWCNT's dosage increased, the adsorption capacity was declining. The main reason is due to the saturation of the adsorption sites with TOC [51].

4.5.3. Effect of solution pH

The initial pH of the solution can have a drastic effect on the adsorption processes in batch processes and can be considered a control parameter in some cases [68]. The variation of pH was found to have varying effects on the adsorption and depends on the pollutant type, as well as the functional groups present on the surface of the adsorbent. For instance, according to [71], the change in pH affected Fe removal using gamma-alumina adsorbent. It was realized that when changing the pH from 4 to 10, the adsorption increased as the pH increased from 4 to 7, but then decreased as pH increased beyond 7. The reason for this trend is explained by competitiveness of the H^+ and OH^- ions with the metal ions in binding with the active site of the gamma-alumina adsorbent surface. Moreover, other studies such as using castor oil and modified castor oil for removal of oil content from PW as proposed by [59], as pH increases, the number of organic compounds that are removed from PW is greater, hence creating more competition with other ions for available adsorption sites, this means that adsorption of oil is more effective at lower pH. Also, in the removal of Sr (II) and Br(II) ions from PW using the AMB [68], it was observed a pH increase resulted in an increase in the adsorption capacity. This is because as the pH decreases, the amount of negative charge on the surface of the AMB increases. This is electrostatically favorable for the Ba (II) and Sr (II) ions and decreases competition with the other ions, therefore, enhances the adsorption process [68]. Thus, there is no trend that can be followed by all the adsorbents regarding pH, since it depends on the interaction of functional groups, adsorbent surfaces and the pollutant characteristics.

4.5.4. Effect of temperature

The effect of temperature on the adsorption process was evaluated for different studies to find if it is exothermic or endothermic in nature. According to studies done by Alatabe et al. for the use of *Imperata cylindrica* for the adsorption of oil, as the temperature increased from 20 to 60 °C, the adsorption capacity increased [56]. Similarly, for lithium adsorption from PW using HMO-2 and HMO-3 [65], an increase in temperature from 20 °C to 70 °C resulted in an increase in lithium adsorbed from 12.5 mg/g to 17 mg/g [65]. These results were justified since the adsorption process was endothermic in nature, and also validated by the evaluation of Gibbs free energy and enthalpy [56,65].

On the contrary, other studies showed that the increase in temperature had the adverse effect on adsorption. For instance, Santos et al. stated that as temperature increases, the adsorption uptake of OGC decreases using CV and CS adsorbents. This justified the absolute value of ΔG decreasing as temperature increases, which indicated a decrease in adsorption and more effectiveness at lower temperatures [61]. Menezes Santos et al. [62] reported that as the temperature increased from 298 to 318 K, the adsorption capacity of OGC for moringa seeds modified with

iron nanoparticles (AC-Fe) from PW decreased. Moreover, using the nanocomposite 3-aminopropyltriethoxysilane functionalised magnetic bentonite (AMB) as adsorbent synthesized by El-Maghrabi et al. [68] in the removal of Sr (II) and Br (II) from PW, it was observed that as temperature increased from 30 °C to 70 °C, the removal percentage of Sr (II) and Br(II) ions decreased. In the removal of TOC from PW using FMWCNTs [51], thermodynamic study revealed that a change in temperature (30–50 °C) resulted in decrease in the adsorption capacity of FMWCNTs. This trend was justified by the high kinetic energy exhibited by the TOC at high temperatures that prevent the TOC from adhering to the surface of adsorbent [51]. In addition, this can also be justified due to the exothermic nature of the adsorption process in all of these examples, and the increasingly negative values of Gibbs free energy, which indicate a decrease in spontaneity with increasing temperatures.

An independent result obtained by Al-Masri et al. [72] for the adsorption of ^{226}Ra onto walnut shell adsorbent, a change in temperature from 15 to 60 °C had insignificant effect on the adsorption percentage of ^{226}Ra in the produced water sample.

4.5.5. Effect of salinity

The effect of salinity of PW on the adsorption process was highlighted in many studies where salinity was measured by varying the concentration of NaCl in the PW. For example, for the removal of emulsified oil from PW using graphene nanoplatelets and graphene magnetite reported by [52], the salinity and initial concentrations of oil affected the removal efficiency; a higher salinity and lower initial concentration of oil increased the efficiency of removal.

However, according to Hendges et al. [7], the change in salinity of the PW was found to have no effect on the adsorption of naphthalic acids (NAs) using MN 202 and L493 adsorbents. Analogous conclusion was drawn from the reports of Menezes Santos et al. when AC-Fe was used for OGC removal from PW. As NaCl concentration varied from 0 to 20 g/L, no significant effect on adsorption was reported [62].

4.6. Fixed bed process

In the study done by Fathy et al. [45], ACTF adsorbent was used for the removal of oil (1000 mg/L) from PW using a fixed bed process. The optimum adsorption (975.43 mg/g) was attained at a feed flowrate of 2.2 ml/min, a bed height of 5 mm, and a breakthrough time of 50 min. The kinetic models used to model the system were Yoon and Nelson and Thomas models, which are based on the Langmuir isotherm model and were used to establish breakthrough curves. The Thomas model exhibited best results, since the regression values (R^2) are closer to 1 [45].

The adsorption of emulsified oil from PW using graphene nanoplatelets and graphene magnetite [52] was studied in continuous operation. Thomas model best fitted the results. The optimum bed height and flowrate that achieved the best adsorption were 2 cm and 0.4 cm/min, respectively and were able to achieve optimal adsorption of 183.4 mg/g using graphene magnetite adsorbent [52].

The use of walnut shell adsorbent for the treatment of PW from ^{226}Ra in a fixed bed adsorption was investigated [72]. Bed height was varied from 5 to 15 cm, and flowrate was varied between 4 and 10 mL/min. Particle size for the adsorbent of 300–425 μm was found to have optimum results for removal, since decreasing the particle size increases the surface area, hence, allows more adsorption. Nevertheless, minute particle sizes of the walnut shell adsorbent are problematic and block the filters during filtration. Thomas model was used to establish the breakthrough curves; this model assumes second-order reversible kinetics [72].

4.6.1. Effect of bed height

In continuous fixed bed processes, the variation of the packing height influences the adsorption process. Increasing the bed height in ACTF fixed bed column [45] increases the adsorption uptake by the adsorbent. This is evident since as the bed height increased from 5 to 15 mm, the percentage of oil removal increased from 26 to 50 %, respectively [45]. Analogous results were obtained from the study by Abou Chacra et al. [52] in packed bed continuous adsorption process using graphene magnetite and nanoplatelets, as the bed height was increased from 1.5 to 2 cm the breakthrough time was found to increase, which is indicative of an increase in adsorption [52]. In another related to the removal of ^{226}Ra ions from PW using walnut shell adsorbent [72], the reported result was similar to the one obtained by [52] which reported a direct relationship between bed height (5 to 15 cm) and the contact time (40 to 100 min). As the amount of adsorbent increased, more time was required to be saturated [72]. This confirms the correlation between height of packing and time required to be saturated with pollutants, since as the number of adsorbent increases, this allows for more active sites and increased capacity of adsorption.

4.6.2. Effect of flowrate

The flowrate of the PW supplied to a fixed bed column influences the adsorption of the pollutant. It was realized that the literature had a unanimous conclusion on the effect of flowrate, and that as the flowrate increased, the adsorption capacity decreases. This was evident in the study by Fathy et al. [45], when the flowrate of water increased from 2.2 mL/min to 8.4 mL/min rapid initial rate of oil adsorption was followed by a slower rate due to the saturation of the pores/active sites. Decreasing the flowrate allowed more time for saturation, since the contact time is greater, and breakthrough time was found to be greater which enhanced the adsorption [45]. Similar results were also obtained by [52]; when the flowrate increased from 0.4 mL/min to 0.8 mL/min, the breakthrough time decreased. This was justified by the decrease in contact time between the adsorbent and PW which resulted in the adsorption of oil. It was reported in the removal of ^{226}Ra ions from PW using walnut shell adsorbent that as the flowrate increased from 4 mL/min to 10 mL/min, the breakthrough time declined from 100 to 65 min. At longer contact times the active sites were saturated by other ions such as Na^+ and Ca^{2+}indicating increased competition with ^{226}Ra [72].

4.7. Adsorption isotherm and kinetic models

4.7.1. Adsorption isotherms

Adsorption isotherm models are valuable tools to quantify the amount of adsorbate an adsorbent can adsorb on its surface, as well as have an understanding on how the pollutant interacts with the adsorbent surface. Isotherm models are also important for comparing the performance of different adsorbents. The non-linear forms of the most prominent adsorption isotherms obtained from several studies are listed in Table 5. It was evident that the most widely used isotherm model for PW adsorption studies was the Langmuir model. Langmuir isotherm model assumes that the adsorption of the adsorbate on the surface occurs in a single layer (monolayer) and that there are fixed and identical adsorption sites [74] with invariable enthalpies [75]. The model also assumed that the adsorbate molecules do not interact, and no steric hindrance is imposed on the system [74].

4.7.2. Adsorption kinetic models

Adsorption kinetic models are important tools that aid in the prediction of equilibrium time of adsorption as well as the rate at which the adsorbate is adsorbed onto the surface. This is vital because modelling the kinetics of adsorption helps not only in enhancing the performance of the adsorbents but also aids the understanding of the adsorption mechanism. The most popularly utilized models are pseudo-first order (PFO) [83], pseudo-second order (PSO) [84] and intra-particle diffusion [85] models, the non-linear form of these models is presented in Table 6. The most prominently applied kinetic model in the adsorption processes is the PSO model. The PSO model assumes that the adsorption of pollutants is second order with respect to available adsorption sites [84].

Kinetic models can also be established for continuous systems and

Table 5
Isotherm models in their non-linear form.

Isotherm	Equation	Parameters	Reference
Langmuir	$q_e = \frac{q_m\, b_0\, C_e}{1 + b_0\, C_e}$	q_e = Equilibrium adsorption capacity (mg/g) q_m = Max. adsorption capacity (mg/g) b_0 = Langmuir constant (L/mg) C_e = Equilibrium conc. of pollutant (mg/L)	[76]
Freundlich	$q_e = k_F\, C_e^{\left(\frac{1}{n}\right)}$	K_F = Freundlich constant (mg/g) (L/g)^n n = Adsorption intensity	[77]
Temkin	$q_e = \frac{R\,T}{b_T} ln(A_T\, C_e)$	R = Universal gas constant (8.314 J/mol. K) T = Temperature (K) b_T = Temkin constant A_T = Temkin binding constant (L/g)	[78]
Toth	$q_e = \frac{k_T\, C_e}{(a_T + C_e)^{\left(\frac{1}{t}\right)}}$	k_T = Toth isotherm constant (mg/g) a_T = Toth isotherm constant (L/mg) t = Toth isotherm constant	[79]
Harkins-Jura	$q_e = \left(\frac{A_H}{B_H - logC_e}\right)\frac{1}{2}$	A_H and B_H = Isotherm constants	[80]
Dubnin-Radushkevich	$q_e = (q_s)\ \exp\ (-k_{ad}^{\varepsilon^2})$	q_S = Theoretical saturation capacity (mg/g) k_{ad} = Dubinin–Radushkevich isotherm constant (mol^2/kJ^2) ε = Dubinin-Radushkevich isotherm constant.	[81]
BET	$q_e = \frac{q_m\, k_{BET}\, C_e}{(C_s - C_e)\left[1 + (k_{BET} - 1)\,\frac{C_e}{C_s}\right]}$	k_{BET} = BET adsorption isotherm relating to energy of surface interaction (L/mg) C_s = Adsorbate monolayer saturation concentration (mg/L)	[82]
Langmuir - BET	$q_e = \frac{q_m\, b_0\, C_e}{1 + b_0\, C_e} + \frac{q_m\, k_{BET}\, C_e}{(C_s - C_e)\left[1 + (k_{BET} - 1)\frac{C_e}{C_s}\right]}$		[7]
Freundlich - BET	$q_e = k_F\, C_e^{\left(\frac{1}{n}\right)} + \frac{q_m\, k_{BET}\, C_e}{(C_s - C_e)\left[1 + (k_{BET} - 1)\frac{C_e}{C_s}\right]}$		

Table 6
Summary of kinetic models used.

Kinetic model	Equation	Parameters	Reference
Pseudo – first order (PFO)	$q_t = q_e - q_e \exp(-k_1\, t)$	q_t = Adsorption capacity (mg/g) k_1 = Rate constant (1/min)	[83]
Pseudo second order (PSO)	$q_t = \frac{q_e^2\, k_2 t}{1 + q_e k_2 t}$	K_2 = PSO rate constant (g/mg. min)	[84]
Intra-particle diffusion	$q_t = k_d t^{1/2} + c$	K_d = Intraparticle diffusion rate constant (mg/g min$^{1/2}$) C = Intercept	[85]

are usually used to form breakthrough curves in order to observe the behavior of the adsorption process and specifically models the concentration of the adsorbate as the solution travels through the column. The most popularly used kinetic models for continuous systems are demonstrated in Table 7 and include the Thomas model [86] and the Yoon and Nelson model [87]. The Thomas model is often referred to as the Bohart-Adams model, which is its correct nomenclature and often there is a confusion in the literature with regards to the naming [88], in this review, wherever it mentions Thomas model it is representative of the Bohart-Adams model.

Table 7
Summary of kinetic models for packed bed column.

Kinetic model	Equation	Parameters	Reference
Thomas	$ln\left(\frac{C}{C_0} - 1\right) = \left(\frac{k_{TH}\, q_e x}{Q}\right) - k_{TH} C_0 V$	k_{TH} = Thomas model constant (ml/min mg) q_e = Anticipated adsorption capacity (mg/g) X = Mass of adsorbent (g) Q = Influent flowrate (ml/min) C_0 = Initial concentration of solution (mg/L) V = Bed volume (ml) C = Concentration of the effluent solution (mg/L)	[86]
Yoon and Nelson	$ln\left(\frac{C}{C_0 - C}\right) = k_{YN} V - \tau k_{YN}$	k_{YN} = Rate constant (min^{-1}) τ = Time required for 50 % breakthrough (min)	[87]

The Bohart Adams model is in fact a special case of the Thomas model neglecting the axial dispersion and rate of following form. The advantage of the Yoon and Nelson model is that no detailed information is required for modelling for the adsorbent or the bed properties which makes it even simpler and more convenient [88]. However, from the studies reviewed for fixed-bed systems, the majority of the adsorbents were modelled using Thomas model (Bohart-Adams model).

4.7.3. Adsorption mechanisms

The adsorption process can occur in many ways depending on the nature of the adsorbent as well as the type of adsorbate. Fig. 5 (A–H) illustrates the different mechanisms [53,89–91] that can possibly occur within adsorption regardless of the type of adsorbent or adsorbate. Moreover, more than one mechanism can be in effect during the adsorption process. In this section, the focus will be on the mechanism of oil adsorption since oil is the main pollutant that is a cause of concern when it comes to treatment of PW.

In Section 4.2, the removal of oil content from PW was discussed, and the effectiveness of adsorbents and operating conditions was mentioned. Few studies evaluated the mechanistic approach of the adsorption process, and if mentioned, it would be very brief. The mechanism of adsorption is usually determined by many methods, most of which are experimental such as: thermodynamic data, spectroscopy, contact angle measurements, point of zero charge measurements, and from kinetic and isotherm models. The adsorbate characteristics also play a role in determination of the adsorption mechanism, in this case oil exhibits hydrophobic characteristics as well as being anionic in nature. Chemisorption is known to be the main adsorption mechanism between the majority of the adsorbents of oil and this was confirmed since most of the oil adsorption processes were chemisorption. But usually, physisorption is preferred due to ease of regeneration, since it is represented by weak forces such as London and Vander Waal forces, while chemically

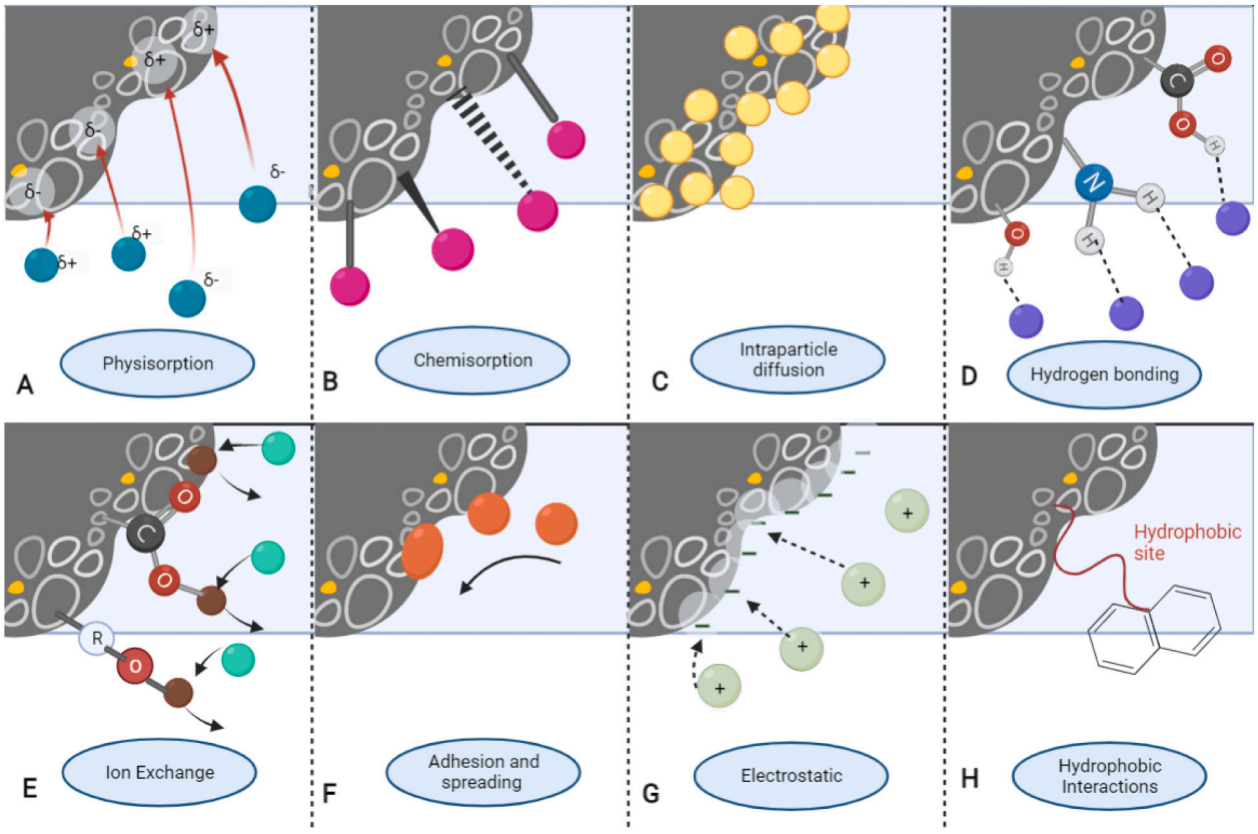

Fig. 5. Illustration of common adsorption mechanisms in the treatment of PW: A) Physisorption, B) Chemisorption, C) Intraparticle diffusion, D) Hydrogen bonding, E) Ion exchange, F) Adhesion and surface spreading, G) Electrostatic, and H) Hydrophobic interactions.

adsorbed particles are harder to be desorbed.

When discussing carbon-based adsorbents such as graphene nanoplatelets, graphene magnetite [52], GIC [53], and CH/PEG/MWCNT [60], it is observed that each of them adsorbs oil content using a different mechanism. Graphene nanoplatelets and graphene magnetite adsorbents was found to adsorb oil via physical adsorption, while GIC's adsorption mechanism was adhesion and spreading (such as shown in Fig. 5 F) and CH/PEG/MWCNT was shown to adsorb oil through chemisorption. The graphene-based adsorbents and the composite CH/PEG/MWCNT's mechanisms were predicted using thermodynamic analyses, specifically the value of relative Gibbs free energy ($\Delta G'$). According to literature, $\Delta G'$ values between −20 to 0 kJ/mol is evident of the physisorption mechanism, while a value from −80 to −400 kJ/mol represents chemisorption [92]. For CH/PEG/MWCNTs, the data correlated better with the pseudo-second order model, and therefore was predicted that the adsorption of oil using this adsorbent was chemisorption [60]. However, for GIC, the mechanism was determined from spectroscopic imaging Cryo-SEM, and it was via adhesion and spreading of the adsorbate particle on to the surface of adsorbent. The spreading of the adsorbate particle is mainly caused by the breaking of the interfacial layer on the adsorbate once it touches the adsorbent surface. Further physicochemical testing such as point of the zero charge on the surface of adsorbate suggested that the interaction of oil and the adsorbent could not have been electrostatic, but rather hydrophobic. This mechanism is also coherent with graphene aerogels, which are novel adsorbents utilized for oil removal [93]. The mechanism under which oil was adsorbed onto this carbon-based adsorbent is through hydrophobic interactions that are enhanced by the graphene structure that acts as a skimmer of oil from water.

Activated carbon (AC) and biochar have been demonstrated to be effective adsorbents of oil for PW treatment. The adsorption of oils and greases using AC prepared from oleifera seeds (CS) and pods (CV) [61] was validated to be of physical nature. This conclusion was reached through thermodynamic analyses, where the enthalpy change was between 0 and −40 kJ/mol. However, this is not enough to reach a verdict about the mechanism of adsorption, since there are many other AC or biochar adsorbents that present a completely different result and suggesting that adsorption of oil on AC or biochar is governed by chemisorption rather than physisorption such as AC-Fe [62], chemically modified moringa oleifera AC [63], and wood derived biochar [94]. FTIR analyses as well as kinetic and isotherm modelling were used to reach those conclusions. On the other hand, AC sourced from petroleum coke for the adsorption of oil from water was shown to be a diffusion-driven process [95]. This is probably due to the hydrogen bonding that hinder the adsorption of oil on pores located on the surface of adsorbent.

Clay-based adsorbents such as Fe_3O_4/Bent NC were able to adsorb oil through chemical bonds between the oil and the adsorbent, which was shown as new peaks on FTIR spectra after adsorption [54]. Moreover, since the adsorption experiments included the addition of surfactant to the oil-water solution, the adsorbate became a surfactant-like structure with a hydrophilic head and hydrophobic tail. This hydrophobic part of the emulsion would facilitate hydrophobic interactions between the emulsion particle and the adsorbent surface. Analogously, the adsorption of dispersed crude oil using montmorillonite, pyrophyllite, kaolinite [96], and organoclay [97] reached the same conclusion; that the adsorption mechanism of oil on clays is governed by hydrophobic interactions between the clay structures and the oil particles and was backed up using the density functional theory (DFT) model. In contrast, since the surface of clays are usually charged (usually positive), there might be a chance that there might be other forces governing the adsorption mechanism such as hydrogen bonding or electrostatic forces [97]. This was verified by Yang et al. when investigating the adsorption mechanism of crude oil on the surface of montmorillonite [98]. This

suggests that the adsorption of oil onto clay adsorbents are governed by three main mechanisms: hydrophobic, electrostatic and hydrogen bonding.

Bio sorbent materials are commonly used and are increasing in population due to their effective adsorptive performance as well as their abundance and cost-effectiveness. *Cassia surattensis* [57] and modified castor oil [59] adsorbents were shown to have a film diffusion mechanism where the adsorption is not dominated by intraparticle diffusion. Not much information was reported regarding the mechanism, and more detailed information is needed for reaching such conclusions. Analogously, an adsorbent synthesized from spent waste rice straw (SWRS) was studied for the removal of oil from wastewater and showed that the adsorption mechanism was not dominated by intraparticle diffusion [99]. Kinetic modelling showed the adsorption following PSO kinetics which indicates the chemisorption of oil particles onto the SWRS, this was backed up with thermodynamic data and FTIR results. In contrast, another rice straw-based bio sorbent demonstrated through zeta potential readings that the mechanism of oil adsorption is facilitated by electrostatic forces [100]. This can be explained, since in batch adsorption experiments for oil, a surfactant is added that makes the emulsion particle positively charged. And with the bio sorbent having a negatively charged surface, electrostatic attraction is the most evident and prominent mechanism. It is rarely reported that the mechanism for oil adsorption using any type of adsorbent is of electrostatic nature, this is because oil is majorly a hydrophobic compound, therefore hydrophobic forces as well as functional groups (chemisorption) are shown to play a major role in the adsorption mechanisms. However, it can be verified that the most common mechanism of oil adsorption was through chemisorption.

4.8. Regeneration and reuse of adsorbents

In order to ensure the cost-effectiveness of the adsorbent in industrial applications, it is vital to understand the feasibility of its desorption and regeneration. There are many methods in which an adsorbent can be regenerated such as thermal regeneration, chemical regeneration, electrochemical regeneration or through novel treatments such as ultrasound and sonication. Effective regeneration of the adsorbent allows for multiple use of adsorbent without compromising the efficiency of pollutant removal.

Abou Chacra et al. [52] regenerated graphene magnetite adsorbent used for emulsified oil removal using n-hexane. The results showed that graphene magnetite was an effective adsorbent that could be regenerated and used again effectively with no changes in efficiency in both continuous and batch processes. Similarly, the regeneration of CH/PEG/MWCNT used for oil removal was carried out by Mottaghi et al. [60] using n-hexane as a desorption medium. Five regeneration cycles (Fig. 2) were carried out under optimum conditions of pH of 3, adsorbent dosage 1 g/L, and oil concentration 1 g/L. It was observed that after each cycle, there was an insignificant decrease in oil capacity as well as negligible weight loss of the adsorbent, this qualifies CH/PEG/MWCNT to be an effective and durable adsorbent to be used for PW treatment [60].

The regeneration of adsorbents is also possible using inorganic chemicals (acids and bases). For instance, in the regeneration of RR-AW reported by Saman et al. [70] which was used in the removal of Hg (II) and MeHg(II) from PW, where 0.1 M KI and 0.1 M HCl solutions were used as eluents and five regeneration cycles were achieved. The efficiency of the adsorbent was not affected with the regeneration of the adsorbent since the initial concentrations of Hg (II) and MeHg (II) were low [71]. Moreover, Hendges et al. [7] studied the desorption of naphthenic acid (NA) from commercial adsorbents MN 202 and L493. The desorption was performed using a basic water solution (1 M NaOH), at different temperatures 25–75 °C, 4 g/L dosage, 4 h contact time. This allowed for complete regeneration of the MN 202 resin at pH 4, initial NA concentration of 200 mg/L, and temperature of 25 °C. Similarly, the desorption and generation of the AC-Fe was also performed using distilled water and 0.1 M HCl solution [62]. The regeneration was done using an adsorbent dose of 0.25 g/L, 200 mL of PW with OGC of 300 mg/L, and three regeneration cycles were performed. It was reported that since the first cycle, the percentage of OGC removal decreased to 66 % using distilled water and 59 % using HCl as a desorption medium. This is due to the blockage of active sites and the chemical and structural changes of the AC-Fe after desorption and regeneration [62]. Magnetic bentonite functionalised with 3-aminopropyltriethoxysilane (AMB) adsorbent regeneration was investigated by El-Maghrabi et al. [68]. The AMB adsorbent was regenerated by eluting it with HCl for three cycles. There was no substantial decrease in adsorption capacities of Sr (II) and Ba (II) after the regeneration. This shows that the AMB adsorbent can successfully be used in PW treatment [68].

Siep et al. [65] investigated the regeneration of manganese-based lithium adsorbents with lithium to manganese ratio of 2:1 (HMO-2) and 3:1 (HMO-3). The desorption using 0.5 M H_2SO_4 for 5 min showed rapid kinetics. After the first cycle of desorption and reuse, the HMO-2 showed the same capacity as the maximum (18 mg/g). However, HMO-3 on the other hand had a significantly lower capacity than the maximum (27 mg/g) which was evidenced by the pH drop that occurred after the regeneration cycle. In addition, after the second cycle, HMO-2 showed a maximum capacity of 16 mg/g and the adsorbent was found agglomerated and floating on the top of the flowback produced water (FPW). This is justified by organic liquids coating the surface of the adsorbent, which could be overcome with the use of surfactant washes after each regeneration cycle before drying [65].

Desorption of the oil saturated walnut shell adsorbent was reported [72] using 0.5 mol/L of NaCl solution acidified with 37 % HCl at a temperature of 60 °C for 3 h. About 31.3 % removal of the ^{226}Ra after triple-washing of the adsorbent was found to completely desorb the ^{226}Ra. The desorbed adsorbent might have undergone Fenton oxidation process in the presence of H_2O_2 and $FeSO_4$ thereby leading to the degradation of oil.

L. He et al. [69] carried out the regeneration and subsequent reuse of the PEG/Fe_3O_4/GO-NH_2 adsorbent. Regeneration of the adsorbent was carried out through sonication and centrifugation while the adsorbent was then reused for the adsorption of calcium and magnesium ions. After the 5th cycle, the reuse rate of the adsorbent was 79.1 % for Ca^{2+} and 69.5 % for Mg^{2+}, while the removal ratios were 69.5 % and 64.3 % for Ca^{2+} and Mg^{2+}, respectively. Core displacement experiments were carried out to show the oil recovery of the PW after the regeneration and was found that after the using PEG/Fe_3O_4/GO-NH_2 as an adsorbent, the oil recovery was improved by 11.8 %. This shows the effectiveness of PEG/Fe_3O_4/GO-NH_2 as an adsorbent for Ca^{2+} and Mg^{2+} removal and post use in oil recovery [69]. In another related study on the thermal regeneration of the PBA-$A^{11.5}U^{12.0}$ adsorbent investigated by Y. Liu et al. [14], the results after 4-cycle thermal treatment showed a decent recyclability and negligible change in the adsorption capacities [14].

For the regeneration process of graphene intercalation compound (GIC) adsorbent using electrochemical processes [53], it was stated that 100 % regeneration efficiency was obtained when using 10 mA/cm^2 current density. The maximum efficiency was reached at contact time of 90 min for the synthetic solution, while it took 4 h to reach maximum removal in the real PW. The longer time to reach maximum removal in the PW was justified by the complexity of PW compared to the synthesized PW. It is expected that side reactions might have taken place. However, an increased voltage can negatively impact the process by corroding the adsorbent and the graphite current feeder. After 5 regeneration cycles, the efficiency was reduced from 100 % to 87 %, which shows that GIC can be effectively used for treatment and regenerated [53].

5. Advanced oxidation process (AOP)

Advanced oxidation processes (AOPs) are part of the chemical treatment that PW undergoes to oxidize the dissolved organic substances

that are too complex to be treated using biological treatment [101]. The oxidation involves the creation of hydroxyl radicals to degrade organic components [102]. The conversion of organic compounds produces safe oxidisable products or causes mineralization of the water [5].

AOPs are shown to be valuable and encouraging methods for PW treatment and allowing for the further reuse and further development of AOPs allows for novel opportunities for the industrial application. On the contrary, AOPs are often costly and require constant maintenance. Moreover, treatment and disposal of by-products is usually very expensive [102]. The drawbacks can be overcome by the development and further studies into AOPs and finding cost effective and innovative methods. Table 8 summarises the different advanced oxidation processes for the removal of several pollutants from PW.

5.1. Fenton oxidation-based -processes

Fenton oxidation was discovered by Henry John Horstman Fenton in 1894 [103], in which he was able to oxidize tartaric acid using hydrogen peroxide (H_2O_2) and ferric ions. The combination of the two Fenton reagents produces hydroxyl radicals (•OH) which has the capability of oxidizing organic pollutants. The following reactions describe the main Fenton mechanism [5]:

$$Fe^{2+} + H_2O_2 \rightarrow Fe^{3+} + \dot{O}H + OH^- \quad (1)$$

$$Fe^{3+} + H_2O_2 \rightarrow Fe^{2+} + H\dot{O}O + H^+ \quad (2)$$

Table 8
Summary of the literature on the degradation of pollutants by advance oxidation process.

AOP type	Pollutant	Initial conc. of pollutant (mg/L)	Conditions	Removal efficiency (%)	Reference
Fenton oxidation	COD	3200	$[H_2O_2]$ = 0.01 mol/L, pH = 3.5, t = 120 min, T = 25 °C, $[H_2O_2]/[Fe^{3+}]$ = 10	91.60	[104]
Photocatalysis (maghemite nanoparticles)	BTEX	600	pH = 3.5, t = 90 min, catalyst concentration = 170 mg/L, UV intensity = 100 W	83	[111]
Photocatalysis (GCN)	Oil	1000	T = 25 °C, 0.20 g photocatalyst, 200 mL solution, t = 60 min in the dark	Visible - 85.4 UV - 96.6	[114]
Photo-electrocatalysis with ozonation (PEC + O_3)	Color	170 PCU (mg Pt-Co/L)	Voltage of photoanode = 2.5 V, t = 120 min, O_3 flowrate = 3.85 × 10^{-4} mol/min, UV irradiation intensity = 36 W, delivered at O_2	98	[118]
	Turbidity	37.2 NTU	flowrate of 3 L/min	100	
	Inorganic carbon	122		99	
	COD	1104		73	
	Fluoride			96	
	Chloride			35	
Electrochemical cell	Sulphide	0.649	Applied potential = 0.5 V (vs. Ag/AgCl), carbon electrodes, t = 2	98	[121]
	TDS	46.01	months	44.79	
	Conductivity	75.9 mS/cm		49.27	
Nano photocatalysis (maghemite nanoparticles)	BTEX	600	T = 25 °C, pH = 3, catalyst conc. = 150 mg/L, visible = 225 W, UV = 100 W, t = 5 days (visible), 90 min (UV)	Visible - 95 % UV - 97	[112]
Photocatalysis	TOC	92	pH = 5, t = 3 h, D = 0.5 g/L P25, irradiance = 250 W/m^2, intensity = 6.5 × 10^{-4} Einstein/min	16	[105]
Fenton oxidation			H_2O_2/COD = 2.1, H_2O_2/Fe = 0.5, T = 20 °C, pH = 3	18	
Photo-Fenton			H_2O_2/COD = 2.1, H_2O_2/Fe = 10, T = 20 °C, pH = 3, t = 2 h, UVC rad (4 × 15 W, λ_{max} = 254 nm, 1.3 × 10^{-4} Einstein/min)	17	
Sono-Fenton			H_2O_2/COD = 2.1, H_2O_2/Fe = 0.5, T = 20 °C, 24 kHz, pH = 3	26	
Ozonation			T = 20 °C, 500 rpm, O_2 = 50 L/h, t = 2 h, O_3 = 1.59–5.7 g/h, 1.5 L reactor	18–24	
Ozonation +H_2O_2			1500 mg/L H_2O_2, pH = 10, 4 g/h O_3, t = 2 h	74	
Electrochemical cell	TOC	350	**Batch:** Current density = 17 mA/cm^2, air flow = 7.3 L/min, pH = 6	97	[123]
	TPH	2300	**Continious:** water flow = 60 ml/min	98	
	Oil and greases	360		95	
Electrochemical cell (Ti/$Ru_{0.3}Ti_{0.7}O_2$ anode)	COD	4600	Current density = 45 mA/cm^2, T = 25 °C, surface area = 18.06 cm^2, time = 5 h, 400 rpm agitation	85	[124]
Nano photocatalysis (γ-Fe_2O_3)	BTEX	600	pH = 3.64, photocatalyst conc. = 167 mg/L, intensity of visible light = 180 W	90.94	[113]
Electrochemical oxidation	COD	960	t = 2 h, CD = 10 mA/cm^2, pH = 4, distance between electrodes = 10 mm	58.60	[125]
Photocatalysis (ZnO/Fe_2O_3 NC)	COD	650	Calcination T = 400 °C, 500 °C, 600 °C, t = variable, conc. = variable	84, 60, 74	[131]
			Conc. = 1 mg/L, 2 mg/L, 3 mg/L, t = variable, T = variable	72, 80, 83	
			Time = 20 min, 100 min, 180 min,T = variable, conc. = variable	44, 72, 82.8	
	Phenol	4.5	Calcination T = 400–600 °C, t = 20–180 min, C = 1–3 mg/L	98.9, 88.9, 69.8	
			Conc. = 1 mg/L, 2 mg/L, 3 mg/L, t = variable, T = variable	76.7, 88.8, 98.7	
			Time = 20 min, 100 min, 180 min, T = variable, C = variable	25.7, 63.5, 97.8	
Ferrate (VI) oxidation	PAHs	1.24911	Ferrate (VI) dosage = 19.35 mg/L, pH = 7.1, t = 68.32 min, T = 25 °C, 250 rpm	89.73	[109]
	COD	2213		73.41	
Ferrate (VI) oxidation	COD	2213	300 mL PW, T = 25 °C, 200 rpm, Fe (VI) dosage = 15 mg/L, t = 50 min, pH = 5	55	[108]
Photoelectrocatalysis	COD	9500	Residence time = 15 min, pH = 3, Applied voltage = 20 V, electrical conductivity = 2500 μS/cm, H_2O_2 = 8 mM, 2 8 W UV lamps	81	[120]
Photocatalytic ozonation (UV-LED/TNA/ozone)	PAHs	0.02371	TNA = 0.2 g/L, 10 UV-LED bulbs 365 nm, t = 1 h, 15 mg O_3/L O_2, Voltage = 34 or 36 V	>90	[6]
Photocatalysis (visible light)	GA	10	200 g/L NaCl, pH = 7, t = 75 min, photocatalyst dosage = 5 g/L	90	[115]
Photocatalysis	Total hydrocarbons	145.9 200–1000	Visible wavelength (400–700 nm), reactor cap = 15 mL and 1 L, 3 W LEDs, V = 3–4 V DC, 700 mA, air supply = 30 L/min at 20 kPa	91.20 98	[116]

$$\dot{O}H + H_2O_2 \rightarrow HOO^{\cdot} + H_2O \quad (3)$$

$$\dot{O}H + Fe^{2+} \rightarrow Fe^{3+} + OH^{-} \quad (4)$$

$$Fe^{3+} + HOO^{\cdot} \rightarrow Fe^{2+} + O_2 + H^{+} \quad (5)$$

$$Fe^{2+} + HOO^{\cdot} + H^{+} \rightarrow Fe^{3+} + H_2O_2 \quad (6)$$

$$HOO^{\cdot} + HOO^{\cdot}(HOO^{\cdot} + O_2 + H^{+}) \rightarrow H_2O_2 + O_2 \quad (7)$$

$$RH + \dot{O}H \rightarrow H_2O + R \rightarrow \text{further oxidation} \quad (8)$$

The Fenton process using H_2O_2 and ferrous sulfate heptahydrate ($FeSO_4.7H_2O$) as Fenton reagents was investigated for treating PW sourced from a Malaysian crude oil facility with initial COD content of 3200 mg/L [104]. The maximum COD removal (91.6 %) was detected at pH 3.5, ratio of hydrogen peroxide to ferric ions $[H_2O_2]/[Fe^{2+}]$ of 10, H_2O_2 concentration of 0.01 mol/L and reaction time of 120 min. They reported that Fenton oxidation was proven to be cost-effective and efficient since it is conducted at room temperature, and no supply of energy is required to commence the reaction. Jiménez et al. [105] also investigated the Fenton oxidation for the removal of TOC (92 mg/L) and COD (262 mg/L) content from synthetic PW. The Fenton oxidation was performed by combination of H_2O_2 and $FeSO_4.7H_2O$, where optimum TOC removal (18 %) was attained at 20 °C and a ratio of $H_2O_2/Fe = 0.5$, $H_2O_2/COD = 2.1$ and pH 3. Distinctly, the Fenton oxidation studied by Afzal et al. [104] had a higher removal percentage of organic content. This can be due to the increased hydrogen peroxide to ferric ions ratio, which can further enhance the adsorption process.

Jiménez et al. [105] attempted to investigate photo-Fenton and sono-Fenton processes for the treatment of synthetic PW from TOC (92 mg/L) and COD (262 mg/L). For the Photo-Fenton process, the same conditions applied to Fenton were used (Table 8), with the addition of UVC radiation (4×15 W, $\lambda_{max} = 254$ nm and intensity of 1.3×10^{-4} Einstein/min). The removal efficiency of TOC enhanced compared with regular Fenton process, since optimal removals were yielded at contact time of 2 h, a H_2O_2/Fe ratio of 10 and a H_2O_2/COD ratio of 2.1, which corresponded to 17 % removal of TOC. Sono-Fenton (combination of sonication and Fenton process) was performed at temperature 20 °C, sonication at a frequency of 24 kHz and acoustic power density of 105 W/cm^2. Sono-Fenton process proved to be better than photo-Fenton and normal Fenton process, which can be justified by increased contact between the free radicals and the organic material, hence, showed better degradation and removal efficiencies. The optimal removal presented using Sono-Fenton was 26 % of TOC, which occurred at a H_2O_2/Fe ratio of 0.5 and H_2O_2/COD of 2.1 [105].

5.2. Ferrate oxidation

Ferrate oxidation is the use of ferric compounds, specifically Fe (VI) for oxidizing organic and inorganic compounds. It is desired for its high oxidation potential, minimal byproduct formation as well as producing end products that are non-toxic [106]. Ferrate oxidation is often used as a pretreatment step prior to membrane processes [107] to avoid the consequences of membrane fouling, however ferrate oxidation has proven to be an effective process on its own. Ferrate oxidation usually follows the following mechanism:

$$FeO_4^{2-} + 8H^{+} + 3e^{-} \rightarrow Fe^{3+} + 4H_2O \quad (9)$$

$$FeO_4^{2-} + 4H_2O + 3e^{-} \rightarrow Fe(OH)_3 + 5OH^{-} \quad (10)$$

$$2FeO_4^{2-} + 5H_2O \rightarrow 2Fe^{3+} + 3/2\ O_2 + 10\ OH^{-} \quad (11)$$

The removal of PAHs and COD from real PW with initial COD and PAH concentration of 2213 mg/L and 1249.11 μg/L was investigated through Ferrate (VI) oxidation [108]. Optimization of the ferrate (VI) oxidation process was performed using CCD based on response surface methodology (RSM) and statistically analyzed using ANOVA. The optimal COD (73.41 %) and PAH (89.73 %) removals from CCD were reported at conditions of pH 7.1, contact time of 68.34 min, ferrate (VI) concentration of 19.35 mg/L, and a temperature of 25 °C. The removal of COD using ferrate oxidation was also conducted by [109]. The optimum removal of COD (55 %) was attained at a temperature 25 °C, pH 5, Fe^{6+} dosage 15 mg/L, and contact time of 50 min. It was observed that an increase in pH from 1 to 5, COD removals increased until it reached maximum, then started to decrease. This was justified by the increase in reactivity of the Fe^{6+} in acidic medium, which increases the amount of degraded organic content. As the Fe (VI) dosage increased, the COD removal increased until it reached a maximum at 15 mg/L, further increase was reported to excessively produce sludge and showed scavenging effects [108]. The two results are comparable since the COD removal attained by [108] was better than of the other, which could be attributed to a higher ferrate concentration that facilitated the degradation of organic content as well as the different pH of the system.

Ferrate oxidation was investigated for the treatment of fracturing wastewater obtained from Daqing oilfield in China to achieve 3 main goals: demulsification, viscosity reduction and COD removal of the fracturing wastewater [110]. The ferrate oxidation was able to increase the demulsification efficiency up to 91.8 %, decrease the viscosity from 1.45 cp to 1.10 cp and achieve a COD removal efficiency of 74.2 %. The addition of the potassium ferrate was able to achieve optimal demulsification efficiency at 45 °C, a ferrate dosage of 5 mg/L, contact time of 4 h, and a pH of 10. Post demulsification, the addition of potassium ferrate was able to achieve optimal COD removal (74.2 %) at a temperature of 40 °C, pH = 10, dosage of 5 mg/L, and 30 min contact time. Post treatment, the treated water's quality was up to standard for reinjection into the oil wells, and therefore enhances the oil recovery [110].

5.3. Photocatalysis

Sheikholeslami et al. [111] used maghemite nanoparticles (γ-Fe_2O_3) for photocatalytic removal of BTEX from PW (Fig. 6). The PW was synthetically prepared with an initial BTEX concentration of 600 mg/L. The maximum removal of BTEX of 83 % occurs at pH 3.5, 90 min contact time, nanoparticle concentration of 170 mg/L and a UV light intensity of 100 W. A later investigation by the same author [112] for photocatalytic

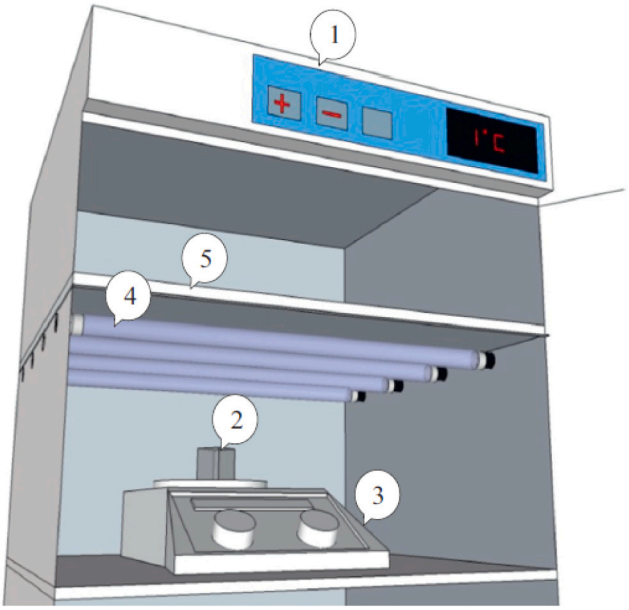

Fig. 6. Experimental set-up: (1) refrigerator, (2) open cubic Plexiglas, (3) stirrer, (4) UV Lamps W [111].

removal of BTEX from PW revealed that 95 % BTEX removal achieved after 5 days for visible and 97 % of BTEX after 90 min for UV (Table 8). It was observed that a reaction utilizing UV light was able to produce faster and more effective results compared to visible light. Implementing the use of γ-Fe_2O_3 on a pilot-scale process was reported by Sheikholeslami et al. [113]. The maximum BTEX (90.94 %) was achieved when operating at temperature 25 °C pH 3.64, photocatalyst concentration of 167 mg/L, and light intensity of 180 W [113]. In comparison with previous studies highlighting the use of maghemite nanoparticles, the authors were able to achieve best BTEX removal results, using visible light. The implementation of this process in industry would be very beneficial especially in the PW treatment field due to its cost effectiveness as well as its adequate performance in BTEX degradation.

The photocatalytic degradation of oil (1000 ppm) in synthetic PW was investigated through graphitic carbon nitride (GCN) as a photocatalyst [114]. The study attempted to compare the performance of direct photolysis (no GCN), GCN, bulk graphitic carbon nitride (b GCN), nanosheets graphitic carbon nitride (nsGCN), PAN nanofibers, NF-bGCN and NF-nsGCN which are bulk and nanosheet graphitic carbon nitride but incorporated with nanofibers. The optimum removal and degradation of oil achieved by the NF-nsGCN was 85.4 % using visible light and 96.6 % using UV light. Three photodegradation cycles were performed using UV radiation, and it was reported that NF-nsGCN could retain 66 % of the original amount, moreover, this was the best result in comparison with PAN and nsGCN [114].

The removal of glutaraldehyde (GA) - a widely used biocide in unconventional oil and gas exploration- from synthetic PW was investigated by Hong et al. [115] using Ag/AgCl/BiOCl as a photocatalyst and visible light. Synthetic PW was synthesized in the lab, had an initial GA concentration of 10 mg/L, salinity of 200 mg/L, and a pH 7. The highest removal of GA (90 %) was observed using the UV irradiation (350 nm), sunlight and visible light (419 nm) at pH 7, 200 g/L NaCl concentration, contact time of 75 min and Ag/AgCl/BiOCl dosage of 5 g/L. Dissolved Organic Carbon (DOC) and Br^- concentrations in the PW were found to hinder the degradation process and affect the efficiency, which could be overcome through increasing the photocatalyst dosage or a greater contact time [115].

To study the removal of organic content (TOC) from PW using titanium oxide (TiO_2) photocatalysis, Velosa-Alfonso et al. [116] modified the TiO_2 with iron oxide (III) and two PW samples were tested: synthesized PW (200–1000 ppm) and one obtained from inlet to a skimmer from a Colombian oil plant (145.9 mg/L). The conditions of operation were at visible light wavelength (400–700 nm), the lighting system had 3 W LEDs as a light source, voltage supplied was from 3 to 4 V, 700 mA current, and air was provided at 20 kPa and 3 L/min. The maximum degradation achieved with TiO_2 photocatalyst are 91.2 % and 98 % for field sample and lab synthesized PW, respectively. This indicates that Fe (III) modified with TiO_2 photocatalyst is an efficient and cost-effective material since the base material (TiO_2) is on hand and abundant, while visible wavelengths (solar irradiation) can also be easily accessed without the need for light circuits installation [116]. Similarly, the commercial photocatalyst Aeroxide ® P25 was utilized for TOC (92 mg/L) and COD (262 mg/L) removal from synthetic PW. The procedure was carried out in a solar simulator (SB) as well as UVA-photo reactor with experimental conditions shown in Table 8. The photocatalysis process was not very effective in the treatment of the produced water even with the addition of an oxidant (H_2O_2) and has presented a maximum TOC removal of 16 % using SB. Compared to other AOPs highlighted in the study, photocatalysis was not as effective in TOC removal [105].

The photocatalytic degradation of BTEX in synthetic PW under visible light using zinc oxide (ZnO) nanorods was attempted by Lin et al. [117]. The system experienced almost 90 % reduction in toluene concentration, approximately 80 % in reduction of ethylbenzene, 65 % reduction in benzene after 3 h. The kinetic model that fit best was the Langmuir-Hinshelwood model, the k_c value was the greatest for toluene k_c = 1.109 mg/L.min, which shows maximum adsorption of toluene. The CO_2 concentration increased as the experiment progressed, this signifies that total mineralization of BTEX and their intermediate products. The regeneration of ZnO nanorods using UV light (Fig. 8) was investigated where 16 cycles were performed. After the 16 cycles, the degradation efficiency of the TB4 and TiO_2 nanosheets were 98 % and 95 % respectively, and it was observed that the photocatalytic activity declined with the constant reuse of the photocatalyst [117]. This suggests that ZnO nanorods could be considered effective photocatalysts for the removal of BTEX from PW, as well as high recyclability and reuse potential.

5.4. Photo electrocatalysis

A comparison between various AOPs including photocatalysis (PC), photo electrocatalysis (PEC), ozonation (O_3) and combined photo electrocatalysis and ozonation (PEC + O_3) for the removal of a variety of pollutants in PW are reported by Brito et al. [118]. Real PW samples obtained from Petrobras; Brazil had initial pollutant concentrations demonstrated in Table 8. The experiments were carried out in an Annular Bubble Reactor (ABR) with two electrodes, the voltage across the electrodes was 2.5 V, the UV irradiation supplied was 36 W supplied, an ozone input rate of 3.85×10^{-4} mol/min and a reaction time of 120 min. The process that yielded the best results was PEC + O_3 and this might be attributed to the incorporation of ozone. The ozone provided a better accessibility for photons to TiO_2 nanotubes thus decreasing the color content. This in turn increased the amount of hydroxyl radicals produced and improved the degradation and removal of the pollutants in PW. The authors reported a significant decrease in the color, turbidity, inorganic carbon, COD, fluoride and chloride concentrations using PEC + O_3. Moreover, conductivity was found to be reduced by 68 %, which was linked to removal of organic carbon by the removal of carbonate ions which are part of the conductivity measurements. Chloride ions were realized to be quite recalcitrant due to the decreased reduction in concentrations [118]. Viana et al. [119] utilized the procedure done by de Brito et al. [118] for the treatment of real PW using 4 different processes was done according to the procedure in by which were photocatalysis, photo electrocatalysis, ozonation and photo electrocatalytic ozonation. The photo electrocatalysis process showed to reduce toxicity of the produced water more effectively where it declared to be a promising treatment process for PW which could be reintroduced back into aquatic systems [119].

Boron carbon nitride (BCN) nanosheets was employed as photo electrocatalysis catalyst [120] using a plug flow (PFR) microreactor to reduce the amount of organic content present as COD in real PW. The PW samples had initial COD and TDS values of 9500 mg/L and 6300 μS/cm respectively. Using the photo electrocatalytic process (microreactor), the greatest COD removal occurred at residence time of 15 min, pH = 3, cell voltage of 20 V, conductivity of 2500 μS/cm and H_2O_2 concentration of 8 mM which corresponded to 81 % COD removal [120]. In contrast with the investigation done by [118] for the combined ozonation and electrocatalysis process, the COD removal was more effective using BCN nanosheets as catalysts, since the reaction time for COD degradation was much less.

5.5. Electrochemical cells

An electrochemical cell was developed and used to reduce the TDS (46.01 g/L) and conductivity (75.9 mS/cm) of synthetic PW [121]. The cell was also used to convert sulfides (0.649 mg/L) into elemental sulfur and caustic soda (NaOH). After applying a temperature of 25 °C, applied potential of 0.5 V (vs. Ag/AgCl) in the cell for 2 months, it was discovered thar maximal removals of TDS (44.79%) and conductivity (49.27%) was achieved. The conductivity (49.27 %). 98 % of the sulfur was converted into other forms such as sulfate (649 mg/L), sulfite (1.027 mg/L), thiosulfate (0.066 mg/L) and polysulfides (423.254 mg/L). It was further discovered that gradual decrease in the sulfide

conversion was due to the sulfur deposition on electrodes which decreased efficiency of conversion. NaOH was directly generated by utilizing the high conductivity of the PW, the cation exchange membrane allows Na^+ to pass, and combines with OH^- to produce NaOH [122]. The amount of NaOH generated was 0.3 g/L. Oxidation of sulfide to elemental sulfur is economically preferred and allows easier separation and recovery of the liquid phase [121].

A novel electrochemical cell (EC) with perforated electrode design was investigated for its effectiveness removal of TOC (350 ppm), total petroleum hydrocarbons (TPH) (2300 ppm), and OGC (360 ppm) from synthetic PW [123]. Five different configurations were tried, but the electrodes with perforated cathode only (Al-PR-C) (Fig. 7) were reported to have the best results in terms of removal, passivation, and power consumption. In addition, the cleaning effect was noticed in which the passive layer peeled off. Optimization using RSM revealed the optimal conditions were at a current density of 17 mA/cm^2, air flow of 7.2 L/min, and pH of 6. Using The EC cell was also tested in continuous operation to see the effect of the geometry and material on the passivation of cathodes for prolonged time of operation. The experiments were carried out at 60 ml/min flow of water, where steady state was reached at 20 min, where 97 % of TOC removal was achieved [123].

In an attempt to investigate different anode materials' effect on the performance of the electrochemical cell in real PW treatment from COD (4600 ppm), three different types of anodes were used: BDD (Boron Doped Diamond), Ti/Pt and Ti/$Ru_{0.3}Ti_{0.7}O_2$ electrodes which are considered active anodes [124]. The removal of COD reported of Ti/$Ru_{0.3}Ti_{0.7}O_2$ (85 %) showed the best removal of COD with conditions shown in Table 8, due to the higher production of active chlorine species that aided in the oxidation of organic compounds. Unlike BDD and Ti/Pt anodes, Ti/$Ru_{0.3}Ti_{0.7}O_2$ exhibited significantly lower concentrations of active chlorine compounds (intermediates) in the effluent as well as lower cost (7.64 USD/m^3) and energy consumption (70 kWh/m^3) [124]. Moreover, electrochemical oxidation of organic content (COD) in real PW was investigated using SnO_2-Sb anode modified with GO (graphene oxide) on titanium substrate, i.e., Ti/Sb-SnO_2 [125]. The best removal of COD was at current density of 10 mA/cm^2, pH of 4, 10 mm between the electrodes, and obtained theoretically 59.96 % removal and energy efficiency of 42.83 g/kWh. However experimentally, 58.6 % COD removal and 42.63 g/kWh energy efficiency were reported. The removal of COD followed PFO kinetics and a rate of 0.005 min $^{-1}$, the COD concentration was not detectible after 235 min. Economic analysis was performed, and

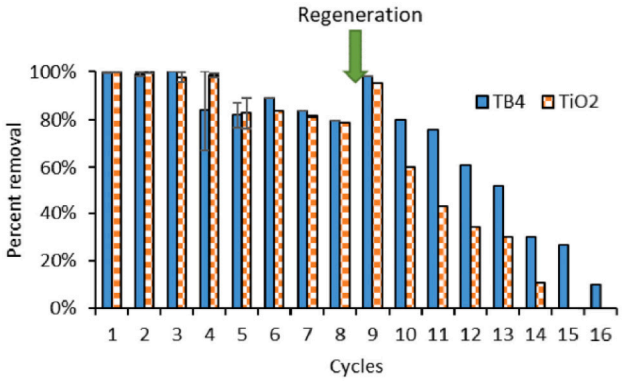

Fig. 8. Ibuprofen removal efficiency of TB4 and TiO_2 catalysts during multiple photocatalytic cycles under UV light irradiation [117].

it was found that the optimized cost is 5.74 USD/m^3 [125]. In terms of cost, the use of Ti/Sb-SnO_2 anodes were able to achieve a lower operational cost than Ti/$Ru_{0.3}Ti_{0.7}O_2$, which is advantageous in the long run and at a macro scale.

5.6. Ozonation

Ozonation process was investigated by Jiménez et al. [105] for synthetic PW treatment using a jacketed boron-glass semi-batch reactor, a temperature of 20 °C, residence time of 2 h, O_2 flow of 50 L/h and ozone flow of 1.59–5.7 g/h, as a result 18–24 % removal of TOC was achieved as an outcome. Combined ozone and H_2O_2 treatment proved to have the best removal of TOC (74 %) at O_3 flow of 4 g/h, 1500 mg/L H_2O_2 concentration, pH of 10, time of 2 h. This corresponded to a TOC in combined H_2O_2 and ozonation process, in which no residual component was produced and, required less electrical energy to degrade the TOC [105]. In another study, B. Liu et al. [6],investigated the photocatalytic ozonation using UV-LED/TNA/ozone for the removal of PAHs (27.31 μg/L) from real PW. The removal of PAHs was found to follow first-order removal kinetics. Ozone was observed to be dominant in the degradation process of the PAHs, since a 30-min treatment at the dosage of 15 mg/L O_2 effectively depleted PAHs. An increase in ozone and catalyst dosage enhanced the removal of PAHs where the optimum amounts were 15

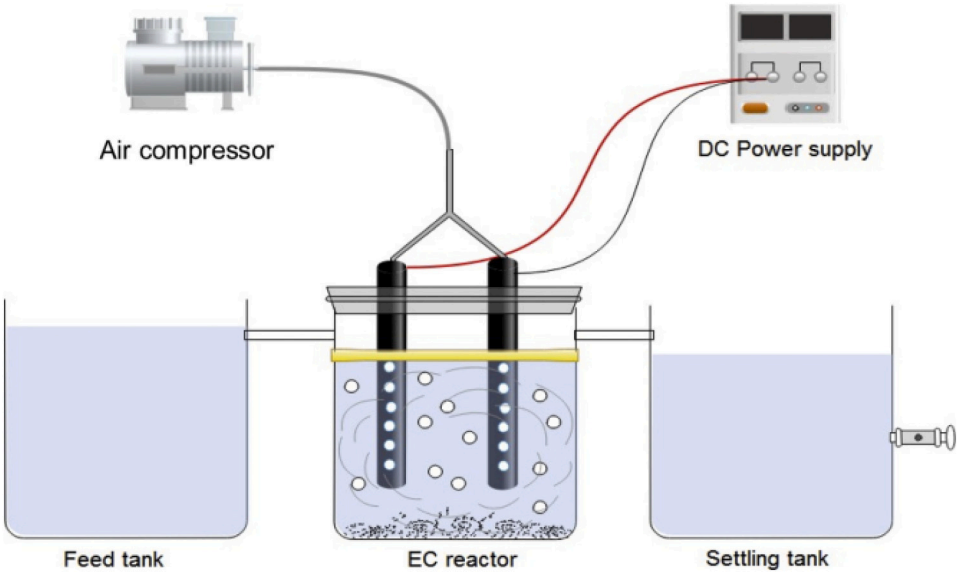

Fig. 7. Schematic diagram of the electrochemical cell setup [123].

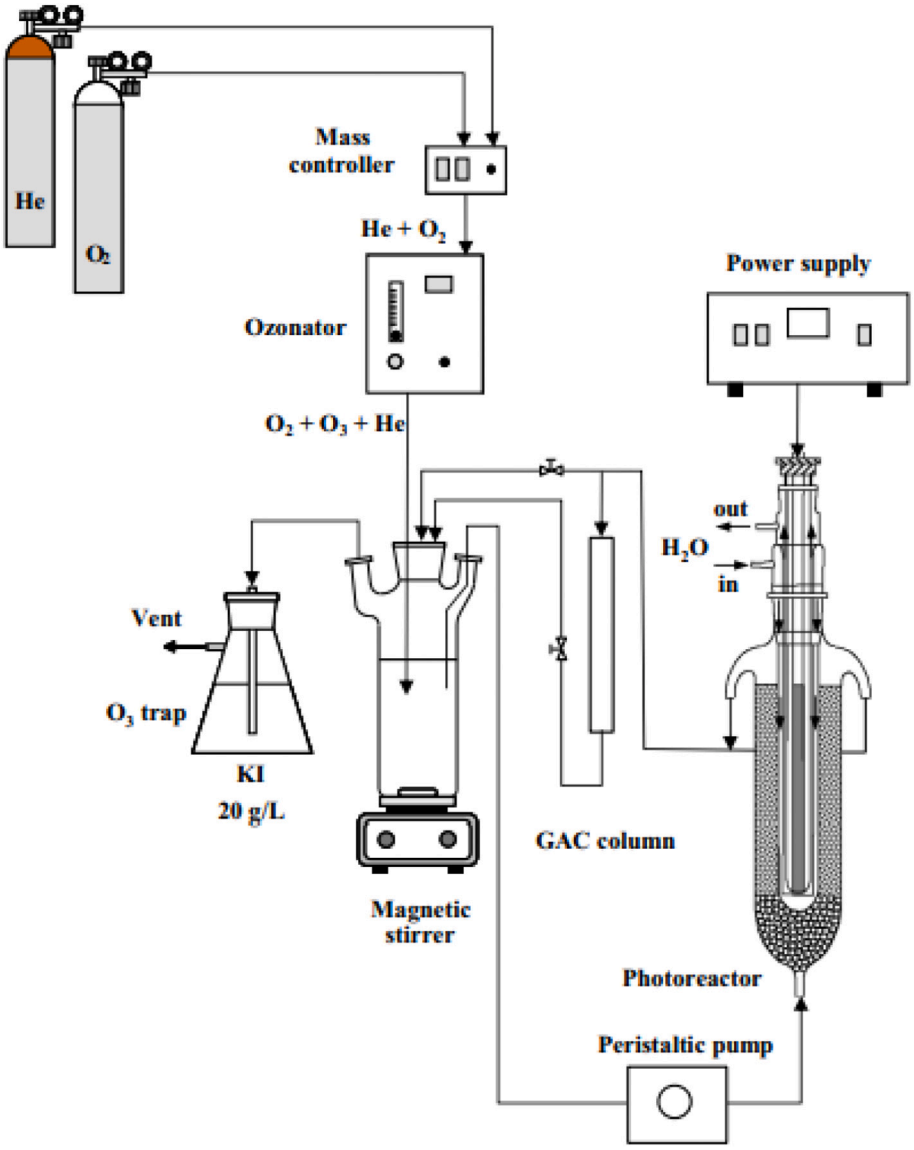

Fig. 9. Combined activated carbon-photocatalysis-ozonation process [136].

mg/L O_2 and 0.2 g/L, respectively. UV irradiation was found to not contribute much to the depletion of PAHs in the first 20 min, however, increasing intensity enhanced the PAH removal at later times [6].

Ozonation of real PW was carried out and targeted the removal of pollutants such as benzene as well as the effectiveness of reducing the toxicity of PW for a possible pre-treatment prior to biological treatment [126]. When ozonation process was compared with electrochemical oxidation and heat-activated persulfate oxidation, it showed the most effective results where it was able to reduce benzene by 71 % and reduce toxicity by 70 % as well as COD and BOD reduction better than the former treatment methods. Ozonation experiments were carried out in a plexiglass column (1 L capacity) at 20°C, where ozone was supplied by an ozone generator and the dosage varied from 3.4 to 151 mg O_3/L. Optimal COD removals were achieved at an ozone dosage of 7.8 mg/L and it was able to reduce toxicity by 40 %, and have achieved 19–71 % removal of BTEX, 46–51 % of propionic acid and complete removal of butyric acid, while the concentration of acetic acid was unchanged, this was attributed to the fact that acetic acid is considered recalcitrant and is difficult to remove from PW. The only drawback of ozonation is the existing of bromide ions in the composition of PW that reacts with ozone and produces harmful by-products. Ozonation was also presented to have the lowest energy consumption corresponding to 0.12 kWh/m^2 in comparison with other treatment processes [126]. This suggests the cost-effectiveness of the ozonation process and the applicability of it as an offshore pre-treatment process.

5.7. Persulfate oxidation

Persulfate oxidation is an effective advanced oxidation technique that utilizes the persulfate ion which can be activated thermally, using UV light and/or acidic pH and can produce free radicals that can aid in the degradation of a variety of pollutants. The electron transfer from transition metals such as iron, manganese and cobalt, and the possible mechanisms are shown using Eqs. (12)–(16) below, the R indicates an organic compound and Me indicates the transition metal.

Persulfate oxidation mechanism [127]:

$$S_2O_8^{2-} \xrightarrow{\text{Heat or UV}} 2SO_4^{\bullet-} \quad k = 1.1 \times 10^{10} \left(\frac{1}{Ms}\right) \tag{12}$$

$$S_2O_8^{2-} + Me^{n+} \rightarrow SO_4^{\bullet -} + Me^{n+1} + SO_4^{2-}\ k = 20\ \left(\frac{1}{Ms}\right) \quad (13)$$

$$SO_4^{\bullet -} + H_2O \rightarrow SO_4^{2-} + OH^{\bullet} + H^{+}\ k = 660\ \left(\frac{1}{s}\right) \quad (14)$$

$$S_2O_8^{2-} + Me^{n+1} \rightarrow S_2O_8^{\bullet -} + Me^{n+1} \quad (15)$$

$$R + Fe^{3+} \rightarrow Fe^{2+} + Products \quad (16)$$

Heat-activated persulfate oxidation of real PW was carried out by [126] using sodium persulfate (SPS) in a 250 mL Erlenmeyer flask that was stirred in a heated magnetic stirring plate. The $Na_2S_2O_8$ dosage was varied from 0.09 to 6.2 g SPS/L while the temperature was varied from 40 to 80 °C. After comparing theoretical and experimental values, the experimental values (19–33 % COD removal) were always 4 times greater than theoretical COD removals (0.5–10 %). However, it is worth noting that a high SPS concentration resulted in undesirable and toxic by-products that were able to destroy microbial activity, this was due to the oxidation by-products formed such as sulfate ions. The best COD removals were found to be at the lowest SPS dosage (89 mg/L) and the greatest temperature (80 °C), where complete consumption was achieved after 5 h [126], this concludes that heat-activated persulfate oxidation is a time- consuming process that depends heavily on the activation temperature and the oxidant dosage. Manz and Carter [128] also investigated the removal of furfural which is a chemical additive used in hydraulic fracturing operations which is found in PW using persulfate oxidation. The activated-persulfate oxidation was carried out using synthesized PW and followed PFO kinetics and the removal was found to be heavily dependent on pH, temperature, persulfate dose, initial iron ion concentration and the presence of other chemical additives. Optimal furfural oxidation using persulfate were achieved at a persulfate dosage of 21 mM, a temperature of 55°C, pH of 5.4 and ferric sulfate concentration of 23.31 mg/L and was able to reduce furfural concentration by >90 % [128].

The removal of many contaminants such as COD and nitrogen ammonium (N-NH4+), were investigated through comparison of electro-activated (EC/PS) and thermal activated (thermal-EC/PS) persulfate oxidation from real PW samples obtained from two different provinces in Iran [129]. The EC/PS process was effective in reducing the H_2S content by 90.1 %, while ammonia levels reached 8 % at optimum conditions which were at neutral pH, 30 min reaction time, PS concentration of 30 mM current density of 35 A/m^2. Thermal activation was performed at an activation temperature of 65°C, the COD removal did not change significantly, but the ammonia concentrations were reduced significantly (69.15 %) and the PS would be activated by thermal instead of by reaction. Comparing the operating costs for EC/PS and thermal/EC/PS, the more cost-effective option is the EC/PS (0.78–1.52 kWh/m3) [129], this is because more electrical energy is required for the provision of heat, which drives the cost of production higher than if it were to be activated by reaction.

Persulfate oxidation using functionalized membranes can be utilized for the removal of organic pollutants such as naphthenic acids (NAs) from synthetic PW [130], where it was effective in reducing the NA content to <10 ppm using an activation energy of 18 kcal/mol (40°C). The process followed PFO kinetics, where a lower concentration of persulfate (500 mg/L) was used to lower the extent of oxidation and avoid membrane immobilization. With the constant reuse of the functionalized membrane, it was realized that the catalytic property of the Fe_xO_y is reduced with each use and turned black/brown color after usage and exposure to persulfate solution, this indicates the oxidation of iron from Fe^{2+} to Fe^{3+}. However, this can be reversed by applying NaBH4 treatment to restore the catalytic property of the membrane. Optimum removals reduced the NA concentrations to 8 mg/L in PW samples using 5000 mg/L of potassium persulfate at 40°C [130].

5.8. The effect of changing different parameters on different AOPs

5.8.1. Fenton-based processes

The effect of changing experimental conditions such as the change in H_2O_2 concentration, reaction time, the hydrogen peroxide to ferric ion ratio and temperature were found to have significant effect on pollutant removal via Fenton-based processes.

The hydrogen peroxide concentration plays a vital role in the performance of the Fenton process as demonstrated in Afzal et al. [104] investigations. It was realized that as the concentration of H_2O_2 increased from 0.12 mmol/L to 0.01 mol/L, the removal of COD has increased from 76 % to 91.6 % respectively. On the contrary, increasing the [H_2O_2] >0.01 mol/L was shown to decrease the COD removal from 91.6 % at 0.01 mol/L to 50 % at 0.1 mol/L. This trend can be justified by higher concentrations of H_2O_2 facilitating the reaction and as it increases, it promotes the generation of the radicals which are responsible for degradation of organic components, however, a further increase in hydrogen peroxide concentration causes the formation of O_2 and causes bubble formation, hence the decrease in COD removal [104].

Increasing the molar ratio of hydrogen peroxide to Fe^{2+} ions from 10 to 25 was shown to present maximum reductions in COD. Normally, an increase in Fe^{2+} ions are associated with the catalyzing of the radical formation reaction, however, in this study it was observed that the Fe^{2+} ions acted as a scavenger and shown to decrease the efficiency of removal as the concentration increased [104].

Contact time is also an important factor in the Fenton process. It was observed that the reaction was very fast in the first 60 min, and it started as soon as the H_2O_2 was added, it was also observed that the optimum COD removal was reached at 120 min [104].

Similar trends were obtained for the investigation performed by Jiménez et al., the effect of temperature was analyzed, and it was found that as the temperature increased from 20 °C to 70 °C, the removal efficiency was enhanced from 18 % to 32 % at the same conditions [105].

5.8.2. Ferrate oxidation

The main parameters that affect the performance of ferrate oxidation were observed to be contact time, pH effect, ferrate (Fe (VI)) dosage, and temperature. The parameter that has the most effect on the ferrate oxidation process was pH, since the ferrate oxidation process is heavily dependent on the initial pH of the solution since the formation of the ferric ions that are responsible for the oxidation are facilitated in acidic environments. The general trend observed across all studies that as the pH increases, the efficiency of the COD removal increases [108–110], however, the values at which optimal removal was achieved varied from one study to the other, but they commonly were greater than pH = 5. As the pH increases from 1 to 7, the COD removal increased until it reached its maximum at pH = 5, this was attributed to the generation of Fe $(OH)_4^-$ and Fe $(OH)_3$ with an increase in pH which decrease the coagulation process [109]. In the removal of COD and PAHs using ferrate oxidation, maximal removal was achieved at pH = 7.5, whereas the pH increased from 5 to 7.5, the removal of COD increased from 45 % to 71.3 %, while the PAH's removal also increased from 67 % to 94.3 %. Moreover, as the pH was increased beyond 7.5, the efficiency of COD and PAH removal decreased, and this was reasoned by ferrate being reduced rapidly in acidic conditions, while it's more stable and degradation is more favorable at higher pHs [108]. During the treatment of fracturing wastewater, as the pH increased from 8 to 10, the demulsification efficiency was enhanced (from 42.5 % to 91.8 %) [110], where the optimal pH that achieved maximum removal of COD and demulsification was at pH = 10.

The Fe (VI) dosage also plays a vital part in the process since it is the main reagent for facilitating the ferric oxide reaction. It was observed that for all studies, as the ferrate dosage increases, the efficiency of pollutant removal also increases [108–110]. The main reason for that is that as the concentration of the ferrate (VI) increases, more Fe^{3+} ions are generated and therefore more pollutant is degraded or decomposed

[107]. However, increasing the dosage beyond the optimal point results in a decreased efficiency of pollutant removal, as well as slows down the reaction, and as a result generates sludge and could have scavenging consequences [109].

It was evident in all studies regarding ferrate oxidation that the more time in contact with the reagent, the greater the removal of pollutants, specifically COD. For both [108,109], the removal of COD increased with increasing contact time and reached its maximum at 50 min, which after that no changes were observed. The reason is that after a long time (50 min), the ferrate ions would be completely degraded and is not able to oxidize and remove any of the pollutants.

Temperature has also been found to affect the pollutant removal and demulsification of oil in fracturing wastewater samples. According to Han et al., 2019, as the temperature increases from 45 to 55 °C, the demulsification efficiency increases until 91.8 %. This is because at higher temperatures, the rate of droplet collision increases between oil particles and results in the break of interfacial film, reduction in viscosity and settling of the oil [110].

5.8.3. Photocatalysis

There are many factors affecting the performance of photocatalysis such as the synthesis properties of the photocatalyst, dosage of photocatalyst, irradiation time and intensity, pH of the initial solution and initial pollutant concentration.

Al Haiqi et al. [131] analyzed factors affecting performance of the nanocomposite in the degradation of COD and phenol, calcination temperature of the nanocomposite, the concentration of ZnO/Fe_2O_3, and the irradiation time, affecting photocatalysis using ZnO/Fe_2O_3 nanocomposite material for the removal of phenol (4.5 mg/L) and COD content (650 mg/L) from PW. As the calcination temperature of photocatalyst increases, the COD and phenol removal efficiencies decrease. An increase in calcination temperature from 400 °C to 600 °C cause the surface area to decrease from 57.64 m^2/g to 7.67 m^2/g and pore volume from 0.137 cm^3/g to 0.078 cm^3/g respectively [131].

Al Haiqi et al. [131] also observed that as the ZnO/Fe_2O_3 concentration increases from 1 to 3 mg/L, the removal of COD increases from 72 to 83 %, while the phenol removal increases from 76.7 to 98.7 %. A similar trend was obtained by [115] for GA removal from PW using Ag/AgCl/BiOCl. However, [111–113] obtained a slightly different trend, as the concentration of the catalyst increases, the pollutant removal efficiency increases, but then decreases again with further increase in concentration. They reported that this was due to the blockage of light due to increased nanoparticle concentration, which in turn diminished the reaction.

Another parameter investigated by [131] was the irradiation time. It was observed that as the irradiation time was kept constant at 20 min, 100 min and 180 min, the COD removal was 44 %, 72 %, and 82.8 %, respectively, while the phenol removal was 25.7 %, 63.5 %, and 97.8 %, respectively. Moreover, according to [111–113] the light intensity was found to majorly affect the removal efficiency, since increasing the light intensity would enhance the rate at which the electrons and holes are formed and in turn, facilitates the COD removal.

Solution pH was found to heavily influence the photocatalytic degradation. Sheikholeslami et al. [111] reported that as the pH increased, the efficiency of COD removal decreased. They observed that pH affects the surface charge and agglomeration affects the catalytic particles at variable pH and added that the isoelectric point or superficial load of the catalyst is influenced by pH changes [112]. On the contrary, [115] reported that an increase in pH enhanced the degradation of GA using the Ag/AgCl/BiOCl photocatalyst. Also, pH alterations presented insignificant effect on the performance of the Aeroxide ® P25 photocatalyst [105].

The presence of some inorganic compounds could influence the removal of pollutants from PW. Jimenez et al. [105] observed that the increased salinity in the PW hindered the TOC removal due to the scavenging effect of the chloride ions on the surface of the TiO_2 photocatalyst surface. A similar trend was also observed in Hong et al.'s investigation for the removal of glutaraldehyde (GA) from PW [115].

5.8.4. Photo-electrocatalysis

The main parameters affecting the performance of photo-electrocatalysis processes used for the treatment of produced water are the initial pH, electrical conductivity of PW, applied cell voltage, hydraulic residence time as well as H_2O_2 concentration.

The effect of changing different parameters was also evaluated thoroughly by [120]. Increasing the pH was found to decrease the COD removal efficiency since the organic compounds were mainly carboxylic acids and phenols that are acidic in nature, so they would be more effectively adsorbed on the surface of photocatalyst in an acidic medium. This was cohesive with the optimum pH condition obtained in the statistical analysis [132] since the optimum pH was found to be pH = 3.3, which is also in the acidic region.

The electrical conductivity/TDS of PW also plays a role in COD removal efficiency. The electrical conductivity can be altered by the addition of salts such as NaCl. According to [120] increasing the PW conductivity from 1100 to 2500 μS/cm was realized to enhance the COD removal from 62.7 % to 80 % as well as accelerate the electro-oxidation process. The reason for this trend is explained by the addition of ions that aided in the electro-oxidation process. However, it was observed that as the conductivity exceeded 2500 μS/cm, the COD removal efficiency was unchanged, and this was due to the competing effects of the scavenging of Cl^- ions as well as photo-oxidation [120].

The cell voltage also plays an important role in determining the effectiveness of the photo electrocatalysis process. According to [120] increasing the cell voltage from 5 to 20 V enhances the COD removal, while further increases in voltage diminish COD removal. The main reason for this trend is that increasing the voltage beyond 20 V, unwanted substances with a negative charge are adsorbed on the surface of the adsorbent, which decreases the COD removal efficiency [120].

Residence time also plays an important role in COD removal, increasing the time from 5 to 15 min increases the COD removal, while at residence time above 15 min causes more competition for the OH^- ions, fewer $OH^•$ produced and therefore decrease in the degradation of organics [120]. These trends were compatible with the optimum residence time obtained by [132] which was 15.85 min and can explain similar trends.

The increase in H_2O_2 concentration was found to affect the performance of the photo electrocatalysis, since it is the main chemical responsible for the production of the hydroxyl radicals that aid in the degradation. An increase in hydrogen peroxide from 4 to 8 mM was shown to increase the COD removal until it reached optimum removal at 8 mM, increase in concentration after that was found to decline COD removal, this can be justified since H_2O_2 generation of hydroxyl radicals is followed simultaneous consumption [120].

According to the statistical analyses performed by [132] for the removal of COD from PW via Photoelectrocatalysis (CCD and Plackett-Burman), the parameters that were of highest influence on the process were the initial pH and the residence time. 7 main parameters were evaluated using the Plackett-Burman design which were initial COD concentration, conductivity of PW, voltage applied, H_2O_2 concentration, residence time and initial pH [132]. The analyses performed by Ebadi et al. [132] were not indicative of the effect of certain parameters on the performance of the process but were just able to determine which parameter had contributed more to the effectiveness of the photo electrocatalysis.

5.8.5. Electrochemical cells

The parameters that affect the performance of electrochemical cells were observed to be current density, initial pH of the electrolyte, distance between electrodes, and the electrode material.

The effect of current density was studied in the electrochemical oxidation using Ti/Sb-SnO_2 anode [125]. It was observed that as the

current density increased the COD removal also increased while similar trends are also reported by Ferreira de Melo et al. [124] in the electrochemical oxidation using 3 different anodes: BDD, Ti/Pt and Ti/$Ru_{0.3}Ti_{0.7}O_2$, as well as in the electrochemical oxidation cell with the perforated electrode [123]. The reason for this behavior was attributed to a higher O_2 diffusion into the anode results in enhanced degradation of the COD content [125]. On the contrary, increasing the current density higher than a certain limit will impact the pollutant removal negatively since the higher current densities, the crystalline structures of the anodes can be irreversibly damaged [125]. Moreover, the higher current densities can also result in undesirable reactions such as the production of chlorine gas that can hinder the degradation process [124]. It was also concluded in other studies such as according to [123] that current density is the most effective parameter that has the most impact on the electrochemical oxidation of the pollutants.

Initial pH of the electrolyte is found to have an effect on the electrochemical oxidation process. According to Pahlevani et al. [125], as the pH increases, the fouling increases, hence, the COD removal percentage decreases and also, at lower pH, the Ti/Sb-SnO_2 anode was found to have a higher oxidative potential and therefore the COD removal is enhanced. Contradictory results were obtained by Ferreira de Melo et al. [124] since at pH >8, the predominant species are ClO^- which increases the chances of radical formation and hence enhanced degradation of pollutants. Differing results were obtained by [123], since the pH did not have much effect on the process, however, the increase in pH beyond 10 (from 10 to 12), the electrolyte presented to increase in viscosity, which could be explained by the initiation of the saponification reaction (formation of soap).

The distance between the electrodes was shown to affect the operation of EO cell, as the distance increased, the COD removal and the energy efficiency increased, however, for energy efficiency 10 mm spacing between the electrodes was shown to enhance the energy efficiency since the electric field strength is higher [123].

The electrode material has an effect on the operation of the electrochemical cell such as in Ferreira de Melo et al.'s [124] observation when 3 anodes were tested for their effectiveness in pollutant removal: boron doped diamond (BDD), Ti/Pt and Ti/$Ru_{0.3}Ti_{0.7}O_2$. The highest removal efficiency was attained by the activated electrodes such as the Ti/$Ru_{0.3}Ti_{0.7}O_2$ (85 %) and Ti/Pt (52 %) as compared with inactivated electrodes such as the BDD (45 %), and the main reason was because of the improved interaction of the surface of the electrode with the (•OH) radicals and therefore an enhanced degradation efficiency. However, in another study, when choosing the material of the electrode between aluminum and iron, aluminum was chosen based on Faraday's law since aluminum has a lower rate of erosion than iron. Moreover, using iron the water turns into a yellowish color due to rust formation. Moreover, aluminum is easier to clean using sand filter compared to iron electrodes [123].

5.8.6. Ozonation

Ozone dosage/concentration supplied to the reactor is realized to be the greatest contributor to pollutant removal using ozonation process which is self-evident. Increasing the ozone dosage presented unanimous results of an increase in pollutant degradation [6,105,126]. According to Jimenez et al. [105], increasing the dosage of ozone from 1.6- to 4.8 g O_3/L enhanced the TOC removal from 33 to 56 %. The main reason for this trend is that long-chain compounds are oxidized which promotes a faster degradation of pollutants [126]. Another reason for this trend is that as ozone concentration increases, the half-life of pollutants such as PAHs is reduced by 2–63 % compared to without ozone [6], which aids in the removal and degradation of such pollutants and at lower reaction times. As much as increasing the ozone supply to the ozonation process is beneficial, the toxicity of the PW after the ozonation process is a persistent issue especially such as in the pre-treatment of PW that is followed by biological treatment [126], the main reason for the insufficient toxicity removals were attributed to incomplete mineralization or incomplete oxidation of biodegradable components of the PW.

In catalytic oxidation [6], the intensity of UV-A as well as the catalyst dosage were shown to impact the degradation and removal of PAHs. The UV-A did not affect the degradation in the initial stages (first 20 min), but at higher light intensities it seemed to impact the degradation of PAHs and showed increased degradation. Moreover, PAHs degradation increased as the catalyst dosage increased where almost all PAHs even those with higher molecular weights were able to completely be degraded after 1 h of operation. However, as catalyst dosage increases beyond the optimal (0.2 g/L), PAH degradation is not that significant due to hydroxyl radical quenchers in the composition of the OPW [6].

The addition of H_2O_2 and Fe^{2+} were explored in the study by Jiménez et al. [105], that showed that the addition of ferric ions was completely unnecessary and negatively impacting due to the consumption of oxygen for the oxidation of iron from Fe^{2+} to Fe^{3+}. Moreover, the formation of such ions causes the formation of sludge which can present another problem of disposal and treatment of the sludge. This was the complete opposite for the addition of H_2O_2, since an increase in H_2O_2 concentration from 557 mg/L to 1500 mg/L has shown improved TOC degradation from 25 % to 33 % [105].

According to Jiménez et al. [105], as initial pH of the solution increases beyond pH = 10, the greater the TOC removal. This can be explained by having more OH^- ions present that enhance the degradation of TOCs as well as the ozone oxidation process being pH dependent.

5.8.7. Persulfate oxidation

The performance of the persulfate oxidation is affected by many parameters such as contact time, temperature, the persulfate reagent dosage, and the pH value.

The temperature was shown to have the greatest effect on the reaction, since most of the time the persulfate is activated thermally (by increasing the temperature). The dominating trend was that as the temperature increases, the degradation of pollutants is also increased this was demonstrated by [126], when the temperature was increased from 65 to 80 °C, the time it took to complete the reaction was reduced by 15 times and suggests that the generation of radicals and eventually the consumption of pollutants was very fast. This can be attributed to one of two main reasons: faster oxidation by the sulfate radicals or unproductive decomposition that generates oxygen, sulfate ions and protons instead [133]. Moreover, according to Manz and Carter [128], the increase in temperature from 20 to 60 °C increases the rate of reaction by 3-fold and this is because as the temperature increases, the persulfate activation is faster.

Persulfate dosage was also an effective parameter in the degradation of pollutants, since as the persulfate dosage increases, the degradation of pollutants also increases. This was demonstrated by Gholami et al. [129], as the dosage increases from 10 to 30 mM, the efficiency increases from 61 to 71 %, and these results were also cohesive with results obtained by [126,128]. However, an increase of the persulfate dosage beyond the optimal values causes scavenging effects and therefore is not always an improvement to the degradation efficiency, as well as the toxic transformation products and the increased level of toxicity that was evident in excess persulfate conditions [126]. In some heat-activated persulfate reactions, iron sulfate is added to catalyse the reaction, and this was evident when the addition of ferric sulfate according to Manz and Carter [128] increased the degradation rate from 10 to 30 %. However, an excess of iron chloride can deplete the persulfate, which puts the need of increasing the dosage of the persulfate even more. Concentrations of iron chloride above the maximum allowable value will react with the persulfate and/or scavenge it and therefore reduces the frequency of the degradation [134].

The pH by which the reaction takes place in plays a major role in the effectiveness and performance of the pollutant degradation by the persulfate oxidation. pH was considered the most important parameter according to Gholami et al. [129], whereas the pH was increased more radicals were produced and therefore the degradation of pollutants

increased, and the main reason was that the free iron ions that would react with the persulfate are less and hence the iron ions would not deplete the persulfate ions. However, for Manz and Carter [128] the opposing scenario was taking place, as the pH was increased, the degradation was decreased, and the highest removal of furfural was achieved at pH of 2.54. Moreover, wells are usually operated at an acidic pH, so having increased efficiency at a lower pH is beneficial for the process to take place effortlessly without the need for any pre-treatment.

6. Adsorption and advanced oxidation integrated process

The use of processes such as adsorption and AOP as single processes was found to be effective in the removal of different pollutants. In treatment of PW, there is no technology that is solely the best to meet the effluent criteria, therefore, the integration of two or more processes can be considered in series or simultaneously [135]. The integration of two or more processes will potentially yield systems that are more cost effective, durable, reusable and the by-products produced are manageable.

Taking the integration of granular activated carbon (GAC) adsorption and photocatalytic oxidation for the removal of 4-Nitrophenol (NP) of a synthetic saline solution, the coupling of these processes has proven to enhance the efficiency of pollutant removal by increasing the reaction rate by 15 % when in comparison with stand-alone processes [136]. The integrated process setup is shown in Fig. 9, where the NP is adsorbed on the GAC surface, then oxidized by the ozone which results in intermediate products, these are then removed by the photocatalytic process. Partial regeneration of the adsorbent (42 %) was observed due to the ozone dissolved, which is advantageous in reducing the cost of maintenance of the adsorption column. TiO_2 photocatalyst was used (Aeroxide P25) operating at room temperature and pressure (T = 25°C and P = 1 atm), bed height of 120 MM, 125 W light intensity, water flowrate of 1.35 cm^3/s. In the ozonation process, the flowrate of ozone supplied was 25 cm^3/min and had a concentration in the liquid phase of 0.084–0.35 ppm. The optimum adsorption conditions were at a flowrate of 6 mL/min and an initial NP concentration of 600 mg/L [136]. Overall, the integrated process was shown to be effective for industrial applications from pollutant removal as well as cost effectiveness perspective.

Wang et al. [137] investigated the treatment of real sample of SGFPW using an integrated oxidation (photocatalysis) and adsorption process (IOAP) for the removal of ammonia nitrogen (NH_3-N) and COD simultaneously using a synthetic zeolite 4A using Xenon lamp (25A) at a zeolite dosage of 10 mg/L, 60 min time and room temperature (25 °C). They reported that the removal of COD and NH_3-N were 59 % and 88.9 %, respectively and the IOAP process was practical due to its economic feasibility and ease of operation [137].

A hybrid photo-Fenton and biosorption using *Phragmites australis* process was studied for the removal of COD (12,654.6 mg/L) and phenol (213 mg/L) from real PW [12]. They reported that for photo-Fenton process, the removals of the COD (69.97 %) and phenol (95.66 %) were obtained at concentration Fe^{2+} of 20 mM, H_2O_2 concentration of 400 mM and a pH of 3.8. The biosorption followed the photo-Fenton, where at the optimum conditions, the maximum capacity of the bio sorbent were 14,421.97 mg/g (69.04 % removal) and 374.90 mg/g (95.8 % removal) for COD and phenol respectively. COD adsorption followed PFO kinetics ($R^2 = 0.999$), while phenol removal followed PSO kinetics ($R^2 = 0.996$). The integration of photo-Fenton and adsorption was found to be a cost-effective process and is a green technology that appears to be promising [12]. The authors did not specify exactly why the integration process has the adsorption process followed by the AOP, but it might be due to the fact that adsorption would make the pollutant available in one place for the AOP to degrade a greater amount of pollutant, and this would also save upon the cost of regeneration of the adsorbent.

A combined process of electro-Fenton and electro sorption operating in continuous system was investigated for the removal of COD, TN, and salinity of a wastewater effluent from a pharmaceutical company which was characterized by high organic content and salinity [138]. The main experimental conditions were a variable voltage from 0.5 to 2.5 V, pH from 3 to 6, spaces between the plates 0.5–2 cm, flowrate of 20–80 mL/min, and H_2O_2 concentration from 0 to 80 mM. The optimal conditions were able to achieve removal efficiencies of 96.5 % COD, 98.2 % of TN, and 46.2 % of salinity. The optimal conditions were attained at voltage of 1.5 V, pH = 4, plate spacing of 1 cm, flowrate of 40 mL/min and hydrogen peroxide concentration of 50 mM. The decrease in salinity was mainly attributed to the electro sorption process. The regeneration and stability of the system was proven to be effective after 5 cycles, moreover, an economic analysis showed that the process was also cost effective and economical and has a cost of operation of $1.18/$m^3$ [138]. This shows that the application of such integrated process is able to effectively remove a variety of pollutants, although this study did not target PW specifically, but since the wastewater was characterized by high salinity and organic content, so this might be applied for PW treatment applications.

7. Future recommendations

From critically analyzing the literature, it was observed that majority of the reported studies were carried out in batch adsorption experiments, but little studies were performed to analyze the performance of the continuous fixed bed adsorption and to establish the breakthrough curves. Therefore, more efforts should be driven toward adsorption fixed-bed adsorption systems. Also, the cost analysis is required for such systems and for the various reported processes used for the regeneration and reuse of the adsorbents.

The effect of salinity is important because PW is very saline and has complex composition. Knowing how these ions and components interact with the adsorbent is vital to understand the adsorption mechanism, and to further enhance the performance of the adsorbents.

Similarly, for AOP, the majority of the reported literature suggested that the use of AOP is promising in the removal of certain pollutants such as organic content, BTEX, oil content and PAHs. However, more studies should be directed toward other pollutants such as phenolic compounds, heavy and toxic metals, as well as chemical additives such as corrosion, scale, and hydrate inhibitors.

More efforts should also be directed into establishment of pilot-scale and scale up of those AOP processes, investigation of cost analysis and energy requirements as well as the management of the byproducts such as the sludge from ferrate oxidation and Fenton processes as well as acetic acid from ozonation process. It was also realized for AOP, that more effort should be put into establishment of a continuous Fenton oxidation system.

With regards to hybridization of adsorption and AOPs, further studies should be carried on evaluating these integrated systems with respect to PW treatment specifically, since most literature provided information regarding industrial wastewater or from food industry wastewater. Moreover, the cost analyses of these systems and possibilities of scale up should be evaluated, as well as comparison of the energy requirements between integrated and standalone processes. Finally, the examination of the effect of the order of either process, which process comes first, or should the system be simultaneously operated, and how would that affect the removal of target pollutants?

8. Conclusion

In this review article, produced water treatment using adsorption and advanced oxidation processes were reviewed and discussed for the removal of different pollutants. The article focused on two main processes: adsorption and advanced oxidation processes and their integration process. Adsorption was proven to be an effective process for the removal of different pollutants such as organic content, oil content, ionic compounds, heavy metals, organic acids and TDS in both batch and fixed

bed systems as well as the regeneration possibilities of certain adsorbents. Furthermore, different types of AOPs such as Fenton oxidation (including Photo-Fenton and Sono-Fenton processes), ferrate oxidation, photocatalysis, photo electrocatalysis, electrochemical cells and ozonation were discussed in this review and different factors affecting the removal of pollutants using these methods are discussed. Finally, the integration of adsorption and advanced oxidation process was found to be competent in the removal of various pollutants. The integration and hybridization of these two processes in forms such as adsorption alongside photo-Fenton, electro Fenton was shown to be more cost effective and efficient than standalone processes.

Abbreviations

AOP	advanced oxidation processes
PW	produced water
WOR	water to oil equivalents
WGR	water to gas equivalents
CBM	coal bed methane
TOC	total organic carbon
BTEX	benzene, toluene, ethylbenzene, xylene
PAHs	polyaromatic hydrocarbons
TDS	total dissolved solids
TSS	total suspended solids
TN	total nitrogen
bbl	barrel
ppm	parts per million
COD	chemical oxygen demand
WS	waste sawdust
MH	moringa husks
AMH	activated moringa husks
TWBC	tea waste biochar
MTWBC	modified tea waste biochar
DOC	dissolved organic carbon
SGFPW	shale gas flowback produced water
PBA	porous biochar aerogel
MWCNT	multiwalled carbon nanotubes
FMWCNT	functionalized multiwalled carbon nanotubes
CCD	central composite design
ACTF	amorphous carbon thin film
GIC	graphite intercalation compound
CS	moringa oleifera seeds
CV	moringa oleifera pods
AC-Fe	moringa oleifera seeds modified with iron nanoparticles
CANa	moringa oleifera pods modified with NaOH
CAH	moringa oleifera pods modified with H_3PO_4
CAZ	moringa oleifera pods modified with $ZnCl_2$
OGC	oil and grease content
LDH	lamellar double hydroxides
FPW	flowback produced water
PU	polyurethane
AMB	3-aminopropyltriethoxysilane functionalised magnetic bentonite
RR-AW	reactive read agrowaste adsorbent
TPH	total petroleum hydrocarbons
RSM	response surface methodology
GCN	graphitic carbon nitride
bGCN	bulk graphitic carbon nitride
nsGCN	nanosheets graphitic carbon nitride
NF-bGCN	bGCN incorporated with nanofibers
NF-nsGCN	nsGCN incorporated with nanofibers
SB	solar simulator
GA	glutaraldehyde
BBDoE	Box Behnken design of experiment
ABR	Annular Bubble Reactor
BCN	boron carbon nitride
PFR	plug flow reactor
OTS	organic total solids
PBA-$A^{11.5}U^{12.0}$	porous biochar aerogel tuned by 11.5 wt% KOH and 12 wt% urea
Fe_3O_2/Bent/NC	iron oxide/bentonite nanocomposite
CH/PEG/MWCNT	chitosan/polyethylene glycol/ multiwalled carbon nanotubes
HMO-2	manganese based lithium adsorbent with Li:Mn ratio of 2:1
HMO-3	manganese based lithium adsorbent with Li:Mn ratio of 3:1
γ-Al_2O_3	gamma alumina
Ec	electrical conductivity
NA	naphthenic acids
PFO	pseudo first order
PSO	pseudo second order
$FeSO_4.7H_2O$	ferrous sulphate heptahydrate
PC	photocatalysis
O_3	ozonation
PEC	photoelectrocatalysis
ZnO	zinc oxide
TiO_2	titanium oxide
NaOH	caustic soda
AL-PR-C	perforated cathode only electrode
EC	electrochemical cells
BDD	boron doped diamond
GO	graphene oxide
GAC	granular activated carbon
NP	4-nitrophenol
IOAP	integrated oxidation and adsorption process
NH_3-N	ammonia nitrogen
H_2O_2	hydrogen peroxide
TOG	total oil and grease

Declaration of competing interest

The authors declare that they have no known competing financial interests or personal relationships that could have appeared to influence the work reported in this paper.

Data availability

No data was used for the research described in the article.

Acknowledgments

This publication was jointly supported by Qatar University and Sultan Qaboos University, Oman, under the international research collaboration grant (IRCC-2021-014; CL/SQU-QU/CESR/21/01). The findings achieved herein are solely the responsibility of the authors. Open Access funding provided by the Qatar National Library.

References

[1] A.A. Olajire, Recent advances on the treatment technology of oil and gas produced water for sustainable energy industry-mechanistic aspects and process chemistry perspectives, Chem. Eng. J. Adv. 4 (2020), 100049, https://doi.org/10.1016/j.ceja.2020.100049.
[2] B.R. Scanlon, R.C. Reedy, P. Xu, M. Engle, J.P. Nicot, D. Yoxtheimer, Q. Yang, S. Ikonnikova, Can we beneficially reuse produced water from oil and gas extraction in the U.S.? Sci. Total Environ. 717 (2020), 137085 https://doi.org/10.1016/j.scitotenv.2020.137085.
[3] C. He, C.P. Harden, Y. Liu, Comparison of water resources management between China and the United States, Geogr. Sustain. 1 (2020) 98–108, https://doi.org/10.1016/j.geosus.2020.04.002.
[4] A. Sadatshojaie, D.A. Wood, S.M. Jokar, M.R. Rahimpour, Applying ultrasonic fields to separate water contained in medium-gravity crude oil emulsions and determining crude oil adhesion coefficients, Ultrason. Sonochem. 70 (2021), 105303, https://doi.org/10.1016/j.ultsonch.2020.105303.
[5] M. Coha, G. Farinelli, A. Tiraferri, M. Minella, D. Vione, Advanced oxidation processes in the removal of organic substances from produced water: potential,

configurations, and research needs, Chem. Eng. J. 414 (2021), https://doi.org/10.1016/j.cej.2021.128668.
[6] B. Liu, B. Chen, B. Zhang, X. Song, G. Zeng, K. Lee, Photocatalytic ozonation of offshore produced water by TiO2 nanotube arrays coupled with UV-LED irradiation, J. Hazard. Mater. 402 (2021), https://doi.org/10.1016/j.jhazmat.2020.123456.
[7] L.T. Hendges, T.C. Costa, B. Temochko, S.Y. Gómez González, L.P. Mazur, B. A. Marinho, A. da Silva, S.E. Weschenfelder, A.A.U. de Souza, S.M.A.G.U. de Souza, Adsorption and desorption of water-soluble naphthenic acid in simulated offshore oilfield produced water, Process. Saf. Environ. Prot. 145 (2021), https://doi.org/10.1016/j.psep.2020.08.018.
[8] A. Alammar, S.-H. Park, C.J. Williams, B. Derby, G. Szekely, Oil-in-water separation with graphene-based nanocomposite membranes for produced water treatment, J. Membr. Sci. 603 (2020), 118007, https://doi.org/10.1016/j.memsci.2020.118007.
[9] S. Jiménez, M.M. Micó, M. Arnaldos, F. Medina, S. Contreras, State of the art of produced water treatment, Chemosphere 192 (2018), https://doi.org/10.1016/j.chemosphere.2017.10.139.
[10] N. Mat Nawi, M. Bilad, G. Anath, N. Nordin, J. Kurnia, Y. Wibisono, N. Arahman, The water flux dynamic in a hybrid forward osmosis-membrane distillation for produced water treatment, Membranes (Basel) 10 (2020) 225, https://doi.org/10.3390/membranes10090225.
[11] H. Mu, Q. Qiu, R. Cheng, L. Qiu, K. Xie, M. Gao, G. Liu, Adsorption-enhanced ceramic membrane filtration using fenton oxidation for advanced treatment of refinery wastewater: treatment efficiency and membrane-fouling control, Membranes (Basel) 11 (2021) 651, https://doi.org/10.3390/membranes11090651.
[12] A. el Shahawy, R.H. Mohamadien, E.M. El-Fawal, Y.M. Moustafa, M.M. K. Dawood, Hybrid Photo-Fenton oxidation and biosorption for petroleum wastewater treatment and optimization using Box–Behnken design, Environ. Technol. Innov. 24 (2021), https://doi.org/10.1016/j.eti.2021.101834.
[13] Y. Dehghani, B. Honarvar, A. Azdarpour, M. Nabipour, Pilot-scale experiments on a hybrid membrane-electrocoagulation system to produced water treatment in a domestic oil reservoir, Water Pract. Technol. 16 (2021) 210–225, https://doi.org/10.2166/wpt.2020.114.
[14] Y. Liu, P. Tang, Y. Zhu, W. Xie, P. Yang, Z. Zhang, B. Liu, Green aerogel adsorbent for removal of organic compounds in shale gas wastewater: high-performance tuning and adsorption mechanism, Chem. Eng. J. 416 (2021), https://doi.org/10.1016/j.cej.2021.129100.
[15] J. Cabrera, M. Irfan, Y. Dai, P. Zhang, Y. Zong, X. Liu, Bioelectrochemical system as an innovative technology for treatment of produced water from oil and gas industry: a review, Chemosphere 285 (2021), 131428, https://doi.org/10.1016/j.chemosphere.2021.131428.
[16] R. Yousef, H. Qiblawey, M.H. El-Naas, Adsorption as a process for produced water treatment: a review, Processes 8 (2020), https://doi.org/10.3390/pr8121657.
[17] C.E. Clark, J.A. Veil, Produced water volumes and management practices in the United States, Argonne, IL (United States) (2009), https://doi.org/10.2172/1007397.
[18] Y. Hedar, Budiyono, Pollution impact and alternative treatment for produced water, E3S Web Conf. 31 (2018), https://doi.org/10.1051/e3sconf/20183103004.
[19] A. Motta, C. Borges, K. Esquerre, A. Kiperstok, Oil produced water treatment for oil removal by an integration of coalescer bed and microfiltration membrane processes, J. Membr. Sci. 469 (2014), https://doi.org/10.1016/j.memsci.2014.06.051.
[20] J. Neff, K. Lee, E.M. DeBlois, Produced water: overview of composition, fates, and effects, in: Produced Water, Springer New York, New York, NY, 2011, https://doi.org/10.1007/978-1-4614-0046-2_1.
[21] P. McCormack, P. Jones, M.J. Hetheridge, S.J. Rowland, Analysis of oilfield produced waters and production chemicals by electrospray ionisation multi-stage mass spectrometry (ESI-MSn), Water Res. 35 (2001), https://doi.org/10.1016/S0043-1354(01)00070-7.
[22] D. Yang, L. Wang, Y. Zhao, Z. Kang, Investigating pilot test of oil shale pyrolysis and oil and gas upgrading by water vapor injection, J. Pet. Sci. Eng. 196 (2021), 108101, https://doi.org/10.1016/j.petrol.2020.108101.
[23] M.S. Mauter, P.J.J. Alvarez, A. Burton, D.C. Cafaro, W. Chen, K.B. Gregory, G. Jiang, Q. Li, J. Pittock, D. Reible, J.L. Schnoor, Regional variation in water-related impacts of shale gas development and implications for emerging international plays, Environ. Sci. Technol. 48 (2014), https://doi.org/10.1021/es405432k.
[24] M. Taulis, M. Milke, Coal seam gas water from Maramarua, New Zealand: characterisation and comparison to United States analogues, J. Hydrol. N. Z. 46 (2007) 1–17. http://www.jstor.org/stable/43944949.
[25] M. Nasiri, I. Jafari, B. Parniankhoy, Oil and gas produced water management: a review of treatment technologies, challenges, and opportunities, Chem. Eng. Commun. 204 (2017), https://doi.org/10.1080/00986445.2017.1330747.
[26] J. Veil, U.S. Produced Water Volumes and Management Practices in 2017, 2020.
[27] Background Review: Co-produced Water - Risks to Aquatic Ecosystems, 2014.
[28] Z.K. Kuraimid, Kh.E. Ahmed, Th.A. Ahmed, L.Y. Abdulla, A.M. al Mesfer, A. Y. Majeed, A.E. Khanfer, M.K. Kitagawa, H.R. Wada, H.I. Isozaki, M.S. Iijima, Sh. O. Oya, T.T. Kanno, Paper title treatment of produced water in North Rumela oil field for re-injection application, in: All Days, SPE, 2013, https://doi.org/10.2118/167670-MS.
[29] A. Hirayama, M. Maegaito, M. Kawaguchi, A. Ishikawa, M. Sueyoshi, A.S. Al-Bemani, A. Mushtaque, H. Esechie, S.A. Al-Mazrui, M.H. Al-Haddabi, S.S. Al-Khanjari, Omani oil fields produced water: treatment and utilization, in: All Days, SPE, 2002, https://doi.org/10.2118/74413-MS.
[30] K. AlAnezi, M. Al-Samhan, M. Belkharchouche, W. Abuhaimed, S. Alali, K. Alenizi, A. Alfuraij, Comparative analysis of produced water collected from different oil gathering centers in Kuwait, J. Environ. Prot. 09 (2018), https://doi.org/10.4236/jep.2018.96046.
[31] Natural Gas Operation, State of Qatar, 2014.
[32] M.A. Al-Ghouti, M.A. Al-Kaabi, M.Y. Ashfaq, D.A. Da'na, Produced water characteristics, treatment and reuse: a review, J. Water Process Eng. 28 (2019), https://doi.org/10.1016/j.jwpe.2019.02.001.
[33] K.L. Benko, J.E. Drewes, Produced water in the Western United States: geographical distribution, occurrence, and composition, Environ. Eng. Sci. 25 (2008), https://doi.org/10.1089/ees.2007.0026.
[34] A. Janson, A. Santos, M. Katebah, A. Hussain, J. Minier-Matar, S. Judd, S. Adham, Assessing the biotreatability of produced water from a Qatari gas field, SPE J. 20 (2015), https://doi.org/10.2118/173188-PA.
[35] A.A. al Haleem, H.H. Abdulah, E.A.-J. Saeed, Components and treatments of oilfield produced water, Al-Khwarizmi Eng. J. 6 (2010) 24–30.
[36] A. Fakhru'l-Razi, A. Pendashteh, L.C. Abdullah, D.R.A. Biak, S.S. Madaeni, Z. Z. Abidin, Review of technologies for oil and gas produced water treatment, J. Hazard. Mater. 170 (2009), https://doi.org/10.1016/j.jhazmat.2009.05.044.
[37] A.M.A. Pintor, V.J.P. Vilar, C.M.S. Botelho, R.A.R. Boaventura, Oil and grease removal from wastewaters: sorption treatment as an alternative to state-of-the-art technologies. A critical review, Chem. Eng. J. 297 (2016), https://doi.org/10.1016/j.cej.2016.03.121.
[38] P.J.C. Tibbetts, I.T. Buchanan, L.J. Gawel, R. Large, A comprehensive determination of produced water composition, in: Produced Water, Springer US, Boston, MA, 1992, https://doi.org/10.1007/978-1-4615-2902-6_9.
[39] J.A. Veil, T.A. Kimmell, A.C. Rechner, Characteristics of produced water discharged to the Gulf of Mexico hypoxiczone, Argonne, IL (United States) (2005), https://doi.org/10.2172/861623.
[40] V.J. Bierman, S.C. Hinz, D. Justic, D. Scavia, J.A. Veil, K. Satterlee, M.E. Parker, J. S. Wilson, Predicted impacts from offshore produced water discharges on hypoxia in the Gulf of Mexico, in: SPE Projects, Facilities & Construction 3, 2008, https://doi.org/10.2118/106814-PA.
[41] M. Hardi, Y.I. Siregar, S. Anita, M. Ilza, Determination of heavy metals concentration in produced water of oil field exploration in siak regency, J. Phys. Conf. Ser. 1156 (2019), https://doi.org/10.1088/1742-6596/1156/1/012009.
[42] I.M. Abou El Leil, K.M. Mezughi, N.M. Triki, S.A. Altayeb, Physiochemical characteristics of produced water in oilfields and its environmental impacts, Int. J. Sci. Dev. Res. 6 (2021) 288–300.
[43] M. Çakmakce, N. Kayaalp, I. Koyuncu, Desalination of produced water from oil production fields by membrane processes, Desalination 222 (2008) 176–186, https://doi.org/10.1016/j.desal.2007.01.147.
[44] S.G. Udeagbara, S.O. Isehunwa, N.U. Okereke, I.U. Oguamah, Treatment of produced water from Niger Delta oil fields using simultaneous mixture of local materials, J. Pet. Explor. Prod. Technol. (2020), https://doi.org/10.1007/s13202-020-01017-w.
[45] M. Fathy, M. El-Sayed, M. Ramzi, O.H. Abdelraheem, Adsorption separation of condensate oil from produced water using ACTF prepared of oil palm leaves by batch and fixed bed techniques, Egypt. J. Pet. 27 (2018), https://doi.org/10.1016/j.ejpe.2017.05.005.
[46] A. Gallo-Cordova, M. del M. Silva-Gordillo, G.A. Muñoz, X. Arboleda-Faini, D. Almeida Streitwieser, Comparison of the adsorption capacity of organic compounds present in produced water with commercially obtained walnut shell and residual biomass, J. Environ. Chem. Eng. 5 (2017), https://doi.org/10.1016/j.jece.2017.07.052.
[47] A.H. Rashid, A.A. Hassan, R.T. Hadi, A.S. Naje, Treatment of oil content in oilfield produced water using chemically modified waste sawdust as biosorbent, Ecol. Environ. Conserv. Pap. 26 (2020) 1563–1571.
[48] A.S.J, T.H. Hussain, A.S. Naje, M.A. Ajeel, Activated carbon prepared from Moringa husks for treatment of oil field produced water, Pollut. Res. 29 (2020) 240–247.
[49] A. Samir, H. Al-Zubaidi, M. Ajeel, A.S.J, A.A. H, Improvement of organic matter removal in water produced of oilfields using low cost Moringa peels as a new green environmental adsorbent, Global NEST J. (2020), https://doi.org/10.30955/gnj.003098.
[50] H. Khurshid, M.R.U. Mustafa, U. Rashid, M.H. Isa, Y.C. Ho, M.M. Shah, Adsorptive removal of COD from produced water using tea waste biochar, Environ. Technol. Innov. 23 (2021), https://doi.org/10.1016/j.eti.2021.101563.
[51] T.L. Adewoye, O.O. Ogunleye, A.S. Abdulkareem, T.O. Salawudeen, J.O. Tijani, Optimization of the adsorption of total organic carbon from produced water using functionalized multi-walled carbon nanotubes, Heliyon 7 (2021), https://doi.org/10.1016/j.heliyon.2020.e05866.
[52] L. Abou Chacra, M.A. Sabri, T.H. Ibrahim, M.I. Khamis, N.M. Hamdan, S. Al-Asheh, M. AlRefai, C. Fernandez, Application of graphene nanoplatelets and graphene magnetite for the removal of emulsified oil from produced water, J. Environ. Chem. Eng. 6 (2018), https://doi.org/10.1016/j.jece.2018.04.060.
[53] Z. Fallah, E.P.L. Roberts, Combined adsorption/regeneration process for the removal of trace emulsified hydrocarbon contaminants, Chemosphere 230 (2019), https://doi.org/10.1016/j.chemosphere.2019.04.224.
[54] D. Ewis, A. Benamor, M.M. Ba-Abbad, M. Nasser, M. El-Naas, H. Qiblawey, Removal of oil content from oil-water emulsions using iron oxide/bentonite nano adsorbents, J. Water Process Eng. 38 (2020), https://doi.org/10.1016/j.jwpe.2020.101583.

[55] H. Albatrni, H. Qiblawey, F. Almomani, S. Adham, M. Khraisheh, Polymeric adsorbents for oil removal from water, Chemosphere 233 (2019), https://doi.org/10.1016/j.chemosphere.2019.05.263.

[56] M.J.A. Alatabe, K.M.M. Al-zobai, H.J. Hadi, Oil removal from produced water using imperata cylindrica as low-cost adsorbent, Curr. Appl. Sci. Technol. 20 (2020) 494–511.

[57] M.K. Ibrahim, A.A. Al-Hassan, A.S. Naje, Utilisation of Cassia surattensis seeds as natural adsorbent for oil content removal in oilfield produced water, Pertanika J. Sci. Technol. 27 (2019) 2123–2138.

[58] A. Saleh Jafer, A.A. Hassan, Removal of oil content in oilfield produced water using chemically modified kiwi peels as efficient low-cost adsorbent, J. Phys. Conf. Ser. (2019) 1294, https://doi.org/10.1088/1742-6596/1294/7/072013.

[59] A.A. Hassan, R.T. Hadi, A.H. Rashid, A.S. Naje, Chemical modification of castor oil as adsorbent material for oil content removal from oilfield produced water, Pollut. Res. Pap. 39 (2020) 892–900.

[60] H. Mottaghi, Z. Mohammadi, M. Abbasi, N. Tahouni, M.H. Panjeshahi, Experimental investigation of crude oil removal from water using polymer adsorbent, J. Water Process Eng. 40 (2021), https://doi.org/10.1016/j.jwpe.2021.101959.

[61] T.M. Santos, F.A. de Jesus, G.F. da Silva, L.A.M. Pontes, Synthesis of activated carbon from oleifera moringa for removal of oils and greases from the produced water, Environ. Nanotechnol. Monit. Manag. 14 (2020), https://doi.org/10.1016/j.enmm.2020.100357.

[62] T. Menezes Santos, J. Valdo da Silva, G. Francisco da Silva, L.A. Magalhães Pontes, Development of a low-cost adsorbent obtained from Moringa Oleifera and functionalized with iron nanoparticles for removal of oil from produced water, Biointerface Res. Appl. Chem. 11 (2021), https://doi.org/10.33263/BRIAC115.1321413231.

[63] M. dos Santos Bispo, J.P.L. dos Santos, L.C.L. dos Santos, L. dos Santos Freitas, D. F. Bispo, G.F. da Silva, Synthesis and characterization of activated carbon of Moringa oleifera Lam pod and evaluation of its performance in the removal of oils and greases, J. Environ. Chem. Eng. 9 (2021), https://doi.org/10.1016/j.jece.2021.105965.

[64] Y. Jang, E. Chung, Lithium adsorptive properties of H2TiO3 adsorbent from shale gas produced water containing organic compounds, Chemosphere 221 (2019), https://doi.org/10.1016/j.chemosphere.2019.01.032.

[65] A. Seip, S. Safari, D.M. Pickup, A.V. Chadwick, S. Ramos, C.A. Velasco, J. M. Cerrato, D.S. Alessi, Lithium recovery from hydraulic fracturing flowback and produced water using a selective ion exchange sorbent, Chem. Eng. J. 426 (2021), https://doi.org/10.1016/j.cej.2021.130713.

[66] B.G.P. Bezerra, A. Parodia, D.R. da Silva, S.B.C. Pergher, Cleaning produced water: a study of cation and anion removal using different adsorbents, J. Environ. Chem. Eng. 7 (2019), https://doi.org/10.1016/j.jece.2019.103006.

[67] M. Ali Syed, M. al Sawafi, F. Shaik, M. Nayeemuddin, Polyurethane green composites: synthesize, characterization and treatment of boron present in the oil produced water, Int. J. Eng. Res. Technol. 13 (2020), https://doi.org/10.37624/IJERT/13.8.2020.1866-1873.

[68] H.H. El-Maghrabi, H.R. Ali, F. Zahran, M.A. Betiha, Functionalized magnetic bentonite-iron oxide nanocomposite and its application to decrease scale formation in tubing of oil/gas production, Appl. Surf. Sci. Adv. 4 (2021), https://doi.org/10.1016/j.apsadv.2021.100058.

[69] L. He, L. Yang, L. Zhang, Z. Wang, H. Cheng, X. Wang, J. Lv, J. Zhang, H. Mo, J. Shen, Removal of Ca2+ and Mg2+ from oilfield wastewater using reusable PEG/Fe3O4/GO-NH2 nanoadsorbents and its efficiency for oil recovery, J. Environ. Chem. Eng. 9 (2021), https://doi.org/10.1016/j.jece.2020.104653.

[70] N. Saman, K. Johari, S.-T. Song, H. Kong, S.-C. Cheu, H. Mat, Enhanced adsorption capacity and selectivity toward inorganic and organic mercury ions from aqueous solution by dye-affinity adsorbents, Environ. Prog. Sustain. Energy 38 (2019), https://doi.org/10.1002/ep.12915.

[71] Z. Karm, A.D. Subhi, R.S. Hamied, Synthesis, characterization and application of gamma-alumina as sorbent material to enhance iron removal from produced water, UPB Sci. Bull. Ser. B: Chem. Mater. Sci. 82 (2020) 237–246.

[72] M.S. Al-Masri, J. Alabdullah, Y. Amin, Y. Al-Khateeb, W. Al-Masri, Y. Aljbai, Treatment of produced water using walnut shell for 226Ra removal, J. Radioanal. Nucl. Chem. 329 (2021), https://doi.org/10.1007/s10967-021-07863-0.

[73] Z. Karm, A.D. Subhi, R.S. Hamied, Comparison study of produced water treatment using electrocoagulation and adsorption, Rev. Chim. 71 (2020), https://doi.org/10.37358/RC.20.11.8370.

[74] K. Vijayaraghavan, T. Padmesh, K. Palanivelu, M. Velan, Biosorption of nickel(II) ions onto Sargassum wightii: application of two-parameter and three-parameter isotherm models, J. Hazard. Mater. 133 (2006) 304–308, https://doi.org/10.1016/j.jhazmat.2005.10.016.

[75] S. Kundu, A.K. Gupta, Arsenic adsorption onto iron oxide-coated cement (IOCC): regression analysis of equilibrium data with several isotherm models and their optimization, Chem. Eng. J. 122 (2006) 93–106, https://doi.org/10.1016/j.cej.2006.06.002.

[76] I. Langmuir, The constitution and fundamental properties of solids and liquids. Part I. Solids, J. Am. Chem. Soc. 38 (1916), https://doi.org/10.1021/ja02268a002.

[77] H.M.F. Freundlich, Over the adsorption in solution, J. Phys. Chem. 57 (1906) 1100–1107.

[78] M. Tempkin, V. Pyzhev, Kinetics of ammonia synthesis on promoted iron catalyst, Acta Phys. Chim. USSR 12 (1940) 327.

[79] J. Toth, State equation of the solid-gas interface layers, Acta Chim. Hung. 69 (1971) 311–328.

[80] W.D. Harkins, G. Jura, Surfaces of solids. XIII. A vapor adsorption method for the determination of the area of a solid without the assumption of a molecular area, and the areas occupied by nitrogen and other molecules on the surface of a solid, J. Am. Chem. Soc. 66 (1944) 1366–1373, https://doi.org/10.1021/ja01236a048.

[81] M. Dubinin, The equation of the characteristic curve of activated charcoal, Dokl. Akad. Nauk SSSR 55 (1947) 327–329.

[82] S. Brunauer, P.H. Emmett, E. Teller, Adsorption of gases in multimolecular layers, J. Am. Chem. Soc. 60 (1938) 309–319, https://doi.org/10.1021/ja01269a023.

[83] S. Lagergren, About the theory of so-called adsorption of soluble substances, in: Kungliga Svenska Vetenskapsakademiens Handlingar 24, 1898, pp. 1–39.

[84] Y.S. Ho, G. McKay, Pseudo-second order model for sorption processes, Process Biochem. 34 (1999) 451–465, https://doi.org/10.1016/S0032-9592(98)00112-5.

[85] J.R. Weber, J. Walter, J.C. Morris, Kinetics of adsorption on carbon from solution, J. Sanit. Eng. Div. 89 (1963) 31–59.

[86] H.C. Thomas, Heterogeneous ion exchange in a flowing system, J. Am. Chem. Soc. 66 (1944) 1664–1666, https://doi.org/10.1021/ja01238a017.

[87] Y.H. Yoon, J.H. Nelson, Application of gas adsorption kinetics I. A theoretical model for respirator cartridge service life, Am. Ind. Hyg. Assoc. J. 45 (1984) 509–516, https://doi.org/10.1080/15298668491400197.

[88] K.L. Tan, B.H. Hameed, Insight into the adsorption kinetics models for the removal of contaminants from aqueous solutions, J. Taiwan Inst. Chem. Eng. 74 (2017) 25–48, https://doi.org/10.1016/j.jtice.2017.01.024.

[89] T.G. Ambaye, M. Vaccari, E.D. van Hullebusch, A. Amrane, S. Rtimi, Mechanisms and adsorption capacities of biochar for the removal of organic and inorganic pollutants from industrial wastewater, Int. J. Environ. Sci. Technol. 18 (2021) 3273–3294, https://doi.org/10.1007/s13762-020-03060-w.

[90] H.N. Tran, S.-J. You, H.-P. Chao, Fast and efficient adsorption of methylene green 5 on activated carbon prepared from new chemical activation method, J. Environ. Manag. 188 (2017) 322–336, https://doi.org/10.1016/j.jenvman.2016.12.003.

[91] S. Ramanayaka, M. Vithanage, A. Sarmah, T. An, K.-H. Kim, Y.S. Ok, Performance of metal–organic frameworks for the adsorptive removal of potentially toxic elements in a water system: a critical review, RSC Adv. 9 (2019) 34359–34376, https://doi.org/10.1039/C9RA06879A.

[92] Y. Yu, Y.-Y. Zhuang, Z.-H. Wang, Adsorption of water-soluble dye onto functionalized resin, J. Colloid Interface Sci. 242 (2001) 288–293, https://doi.org/10.1006/jcis.2001.7780.

[93] W. Kang, Y. Cui, L. Qin, Y. Yang, Z. Zhao, X. Wang, X. Liu, A novel robust adsorbent for efficient oil/water separation: magnetic carbon nanospheres/graphene composite aerogel, J. Hazard. Mater. 392 (2020), 122499, https://doi.org/10.1016/j.jhazmat.2020.122499.

[94] X. Zhou, L. Shi, T.B. Moghaddam, M. Chen, S. Wu, X. Yuan, Adsorption mechanism of polycyclic aromatic hydrocarbons using wood waste-derived biochar, J. Hazard. Mater. 425 (2022), 128003, https://doi.org/10.1016/j.jhazmat.2021.128003.

[95] M. Yuan, S. Tong, S. Zhao, C.Q. Jia, Adsorption of polycyclic aromatic hydrocarbons from water using petroleum coke-derived porous carbon, J. Hazard. Mater. 181 (2010) 1115–1120, https://doi.org/10.1016/j.jhazmat.2010.05.130.

[96] J.A. Greathouse, R.T. Cygan, J.T. Fredrich, G.R. Jerauld, Adsorption of aqueous crude oil components on the basal surfaces of clay minerals: molecular simulations including salinity and temperature effects, J. Phys. Chem. C 121 (2017) 22773–22786, https://doi.org/10.1021/acs.jpcc.7b06454.

[97] J.M. Younker, M.E. Walsh, Impact of salinity and dispersed oil on adsorption of dissolved aromatic hydrocarbons by activated carbon and organoclay, J. Hazard. Mater. 299 (2015) 562–569, https://doi.org/10.1016/j.jhazmat.2015.07.063.

[98] Z. Yang, S. Fang, M. Duan, Y. Xiong, X. Wang, Chemisorption mechanism of crude oil on soil surface, J. Hazard. Mater. 386 (2020), 121991, https://doi.org/10.1016/j.jhazmat.2019.121991.

[99] H.N. Nassar, W.I.M. El-azab, N.Sh. El-Gendy, Sustainable ecofriendly recruitment of bioethanol fermentation lignocellulosic spent waste biomass for the safe reuse and discharge of petroleum production produced water via biosorption and solid biofuel production, J. Hazard. Mater. 422 (2022), 126845, https://doi.org/10.1016/j.jhazmat.2021.126845.

[100] L. Feng, Y. Gao, Z. Dai, H. Dan, F. Xiao, Q. Yue, B. Gao, S. Wang, Preparation of a rice straw-based green separation layer for efficient and persistent oil-in-water emulsion separation, J. Hazard. Mater. 415 (2021), 125594, https://doi.org/10.1016/j.jhazmat.2021.125594.

[101] S. Dave, J. Das, Technological model on advanced stages of oxidation of wastewater effluent from food industry, in: Advanced Oxidation Processes for Effluent Treatment Plants, Elsevier, 2021, https://doi.org/10.1016/B978-0-12-821011-6.00002-5.

[102] W.F. Elmobarak, B.H. Hameed, F. Almomani, A.Z. Abdullah, A review on the treatment of petroleum refinery wastewater using advanced oxidation processes, Catalysts 11 (2021), https://doi.org/10.3390/catal11070782.

[103] H.J.H. Fenton, Oxidation of tartaric acid in presence of iron, J. Chem. Soc. Trans. 65 (1894) 899–910.

[104] T. Afzal, M.H. Isa, M. Raza ul Mustafa, Removal of organic pollutants from produced water using Fenton oxidation, E3S Web Conf. 34 (2018), https://doi.org/10.1051/e3sconf/20183402035.

[105] S. Jiménez, M. Andreozzi, M.M. Micó, M.G. Álvarez, S. Contreras, Produced water treatment by advanced oxidation processes, Sci. Total Environ. 666 (2019), https://doi.org/10.1016/j.scitotenv.2019.02.128.

[106] C. Bustillo-Lecompte, Advanced Oxidation Processes - Applications, Trends, and Prospects, IntechOpen, 2020, https://doi.org/10.5772/intechopen.85681.

[107] P. Tang, W. Xie, A. Tiraferri, Y. Zhang, J. Zhu, J. Li, D. Lin, J.C. Crittenden, B. Liu, Organics removal from shale gas wastewater by pre-oxidation combined with

biologically active filtration, Water Res. 196 (2021), 117041, https://doi.org/10.1016/j.watres.2021.117041.
[108] T. Haneef, M.R. Ul Mustafa, K.W. Yusof, M.H. Isa, M.J.K. Bashir, M. Ahmad, M. Zafar, Removal of polycyclic aromatic hydrocarbons (PAHs) from produced water by ferrate (VI) oxidation, Water (Basel) 12 (2020), https://doi.org/10.3390/w12113132.
[109] T. Haneef, M.R. Ul Mustafa, F.H.M. Yasin, S. Farooq, M., Hasnain Isa, Study of Ferrate(VI) oxidation for COD removal from wastewater, IOP Conf. Ser. Earth Environ. Sci. 442 (2020), https://doi.org/10.1088/1755-1315/442/1/012007.
[110] H. Han, J. Li, Q. Ge, Y. Wang, Y. Chen, B. Wang, Green Ferrate(VI) for multiple treatments of fracturing wastewater: demulsification, visbreaking, and chemical oxygen demand removal, Int. J. Mol. Sci. 20 (2019) 1857, https://doi.org/10.3390/ijms20081857.
[111] Z. Sheikholeslami, D. Yousefi Kebria, F. Qaderi, Nanoparticle for degradation of BTEX in produced water; an experimental procedure, J. Mol. Liq. 264 (2018), https://doi.org/10.1016/j.molliq.2018.05.096.
[112] Z. Sheikholeslami, D. Yousefi Kebria, F. Qaderi, Investigation of photocatalytic degradation of BTEX in produced water using γ-Fe2O3 nanoparticle, J. Therm. Anal. Calorim. 135 (2019), https://doi.org/10.1007/s10973-018-7381-x.
[113] Z. Sheikholeslami, D.Y. Kebria, F. Qaderi, Application of γ-Fe2O3 nanoparticles for pollution removal from water with visible light, J. Mol. Liq. 299 (2020), https://doi.org/10.1016/j.molliq.2019.112118.
[114] N.H. Alias, J. Jaafar, S. Samitsu, N. Yusof, M.H.D. Othman, M.A. Rahman, A. F. Ismail, F. Aziz, W.N.W. Salleh, N.H. Othman, Photocatalytic degradation of oilfield produced water using graphitic carbon nitride embedded in electrospun polyacrylonitrile nanofibers, Chemosphere 204 (2018), https://doi.org/10.1016/j.chemosphere.2018.04.033.
[115] S. Hong, T. Ratpukdi, B. Sungthong, J. Sivaguru, E. Khan, A sustainable solution for removal of glutaraldehyde in saline water with visible light photocatalysis, Chemosphere 220 (2019), https://doi.org/10.1016/j.chemosphere.2018.12.216.
[116] P.C. Velosa-Alfonso, Andrés Felipe Loaiza-Carreño, C.A. Quiñones-Segura, Photocatalytic degradation of hydrocarbons present in water, using Fe (III) modified TiO2, CT&F Cienc. Tecnol. Futuro 9 (2019), https://doi.org/10.29047/01225383.156.
[117] L. Lin, W. Jiang, M. Bechelany, M. Nasr, J. Jarvis, T. Schaub, R.R. Sapkota, P. Miele, H. Wang, P. Xu, Adsorption and photocatalytic oxidation of ibuprofen using nanocomposites of TiO2 nanofibers combined with BN nanosheets: degradation products and mechanisms, Chemosphere 220 (2019), https://doi.org/10.1016/j.chemosphere.2018.12.184.
[118] J.F. Bde Brito, G.G. Bessegato, P.R.F. Tde Toledo e Souza, T.S. Viana, D.P. de Oliveira, C.A. Martínez-Huitle, M.V.B. Zanoni, Combination of photoelectrocatalysis and ozonation as a good strategy for organics oxidation and decreased toxicity in oil-produced water, J. Electrochem. Soc. 166 (2019), https://doi.org/10.1149/2.0331905jes.
[119] T.S. Viana, T.C.R. Rialto, J.F.D. Brito, A.F.D. Micas, F.R. Abe, E.A. Savazzi, M.V. B. Boldrin Zanoni, D.P. de Oliveira, Effects of water produced by oil segment on aquatic organisms after treatment using advanced oxidative processes, J. Toxic. Environ. Health A 84 (2021) 901–913, https://doi.org/10.1080/15287394.2021.1951910.
[120] S. Ebadi, K. Ghasemipanah, E. Alaie, A. Rashidi, A. Khataee, COD removal from gasfield produced water using photoelectrocatalysis process on coil type microreactor, J. Ind. Eng. Chem. 98 (2021), https://doi.org/10.1016/j.jiec.2021.03.045.
[121] P. Jain, S. Srikanth, M. Kumar, P.M. Sarma, M.P. Singh, B. Lal, Electrochemical sulfur production from treating petroleum produced water, J. Water Process Eng. 28 (2019), https://doi.org/10.1016/j.jwpe.2019.01.020.
[122] I. Pikaar, R.A. Rozendal, Z. Yuan, K. Rabaey, Electrochemical caustic generation from sewage, Electrochem. Commun. 13 (2011), https://doi.org/10.1016/j.elecom.2011.08.044.
[123] M.H. Ibrahim, D.T. Moussa, M.H. El-Naas, M.S. Nasser, A perforated electrode design for passivation reduction during the electrochemical treatment of produced water, J. Water Process Eng. 33 (2020), https://doi.org/10.1016/j.jwpe.2019.101091.
[124] J. Ferreira de Melo, D. Medeiros de Araújo, D. Ribeiro da Silva, C. Alberto Martinez Huitle, P. Villegas-Guzman, Applicability of electrochemical technology for treating a real petrochemical effluent by electro-generated active chlorine species, Int. J. Electrochem. Sci. 15 (2020), https://doi.org/10.20964/2020.10.66.
[125] L. Pahlevani, M.R. Mozdianfard, N. Fallah, Electrochemical oxidation treatment of offshore produced water using modified Ti/Sb-SnO2 anode by graphene oxide, J. Water Process Eng. 35 (2020), https://doi.org/10.1016/j.jwpe.2020.101204.
[126] A.R. Ferreira, L. Breinholt, K.M.S. Kaarsholm, D.F. Sanchez, R.K. Chhetri, J. Muff, H.R. Andersen, Feasibility study on produced water oxidation as a pretreatment at offshore platform, Process. Saf. Environ. Prot. 160 (2022) 255–264, https://doi.org/10.1016/j.psep.2022.02.008.
[127] C. Liang, C.-P. Liang, C.-C. Chen, pH dependence of persulfate activation by EDTA/Fe(III) for degradation of trichloroethylene, J. Contam. Hydrol. 106 (2009) 173–182, https://doi.org/10.1016/j.jconhyd.2009.02.008.
[128] K.E. Manz, K.E. Carter, Investigating the effects of heat activated persulfate on the degradation of furfural, a component of hydraulic fracturing fluid chemical additives, Chem. Eng. J. 327 (2017) 1021–1032, https://doi.org/10.1016/j.cej.2017.06.168.
[129] M. Gholami, B. Abbasi Souraki, A. Pendashteh, Electro-activated persulfate oxidation (EC/PS) for the treatment of real oilfield produced water: optimization, developed numerical kinetic model, and comparison with thermal/EC/PS and EC systems, Process. Saf. Environ. Prot. 153 (2021) 384–402, https://doi.org/10.1016/j.psep.2021.07.011.
[130] A. Aher, J. Papp, A. Colburn, H. Wan, E. Hatakeyama, P. Prakash, B. Weaver, D. Bhattacharyya, Naphthenic acids removal from high TDS produced water by persulfate mediated iron oxide functionalized catalytic membrane, and by nanofiltration, Chem. Eng. J. 327 (2017) 573–583, https://doi.org/10.1016/j.cej.2017.06.128.
[131] O. Al Haiqi, A. Hamid Nour, B.V. Ayodele, R. Bargaa, Interaction effect of process variables on solar-assisted photocatalytic phenol degradation in oilfield produced water over ZnO/Fe2O3 nanocomposites, J. Adv. Res. Fluid Mech. Therm. Sci. 78 (2020), https://doi.org/10.37934/arfmts.78.1.100121.
[132] S. Ebadi, K. Ghasemipanah, E. Alaie, A. Rashidi, A. Khataee, Using BCN nanostructure as anode electrode for photoelectrocatalytic degradation of organics: a statistical approach, J. Water Supply Res. Technol. AQUA 70 (2021) 856–867, https://doi.org/10.2166/aqua.2021.034.
[133] C.M. Dominguez, A. Checa-Fernandez, A. Romero, A. Santos, Degradation of HCHs by thermally activated persulfate in soil system: effect of temperature and oxidant concentration, J. Environ. Chem. Eng. 9 (2021), 105668, https://doi.org/10.1016/j.jece.2021.105668.
[134] I.M. Kolthoff, A.I. Medalia, H.P. Raaen, The reaction between ferrous iron and peroxides. IV. Reaction with potassium persulfate [1a], J. Am. Chem. Soc. 73 (1951) 1733–1739, https://doi.org/10.1021/ja01148a089.
[135] M. Golestanbagh, M. Parvini, A. Pendashteh, Integrated systems for oilfield produced water treatment: the state of the art, Energy Sources Part A 38 (2016), https://doi.org/10.1080/15567036.2016.1154903.
[136] S. Cataldo, A. Iannì, V. Loddo, E. Mirenda, L. Palmisano, F. Parrino, D. Piazzese, Combination of advanced oxidation processes and active carbons adsorption for the treatment of simulated saline wastewater, Sep. Purif. Technol. 171 (2016) 101–111, https://doi.org/10.1016/j.seppur.2016.07.026.
[137] M. Wang, L. He, M. Wang, L. Chen, S. Yao, W. Jiang, Y. Chen, Simultaneous removal of NH3-N and COD from shale gas distillate via an integration of adsorption and photo-catalysis: a hybrid approach, J. Environ. Manag. 249 (2019), https://doi.org/10.1016/j.jenvman.2019.109342.
[138] Y. Chai, P. Qin, Z. Wu, M. Bai, W. Li, J. Pan, R. Cao, A. Chen, D. Jin, C. Peng, A coupled system of flow-through electro-Fenton and electrosorption processes for the efficient treatment of high-salinity organic wastewater, Sep. Purif. Technol. 267 (2021), https://doi.org/10.1016/j.seppur.2021.118683.